CHALMERS
UNIVERSITY OF TECHNOLOGY

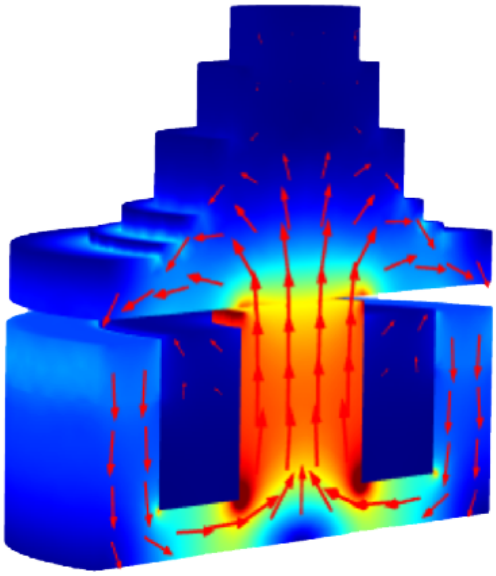

Electromechanical Simulation for Transducers in Bone Anchored Hearing Systems

Thesis work for the Department of Electrical Engineering together with Oticon Medical.

DANNY MESSINGER and ALEXANDER VANNAS

Department of Electrical Engineering
CHALMERS UNIVERSITY OF TECHNOLOGY
Gothenburg, Sweden 2020

Master's thesis 2020

Electromechanical Simulation for Transducers in Bone Anchored Hearing Systems

Thesis work for the department of electrical engineering together with Oticon Medical AB.

DANNY MESSINGER AND ALEXANDER VANNAS

CHALMERS
UNIVERSITY OF TECHNOLOGY

Department of Electrical Engineering
Chalmers University of Technology
Gothenburg, Sweden 2020

Electromechanical Simulation for Transducers in Bone Anchored Hearing Systems
DANNY MESSINGER and ALEXANDER VANNAS

Supervisor: Tomas Johansson, Oticon Medical AB
Examiner: Sabine Reinfeldt, Department of Electrical Engineering, Chalmers University of Technology

Master's Thesis 2020 Department of Electrical Engineering
Chalmers University of Technology
SE-412 96 Gothenburg
Telephone +46 31 772 1000

Cover: Cross section of an electromagnetic simulation of a transducer for bone anchored hearing system.

Typeset in LaTeX
Gothenburg, Sweden 2020

Abstract

The World Health Organization estimates that hearing loss is affecting around 466 million people around the world and the progression over time is increasing. Various types of hearing loss can be treated using a bone anchored hearing system (BAHS). A BAHS redirects the sound waves via vibrations through the skull bone to the cochleae where the signals are further transferred to the brain. Several BAHS exists on the market today, where Oticon Medical AB is one producer. The BAHS can be viewed as a spring mass system with an electromagnetic motor that generates vibrations.

The aim of this thesis was to create a simulation environment for an Oticon Medical Transducer (OMT). The study focused on the magnetic flux in the OMT, which is an electromagnetic transducer, and the force output that is generated from the system. The aim was also to present some optimization of the OMT in regards to saturation and material properties extracted from the simulations.

There are multiple ways to simulate an electromechanical model. This thesis is using COMSOL Multiphysics as a simulation software. In order to fulfill the aim, four different cases were developed. The first case was individually testing of the mechanical spring, the electromagnetic coil and the permanent magnet of the OMT. The second case was to perform a stationary analysis of the assembled transducer. The third case consisted of a time and frequency analysis of the OMT, while the fourth case compared three different properties: the force output of different air gaps, the force output change in regards to permeability and force output variation in regards to the magnetization vector.

The results of the first two cases were verified using reference measurements. When analyzing case 3, a difference between the measurement, and the simulation was initially found. In order to match the measurements five parameters were changed to alter the behavior of the simulation. These parameters are the air gap of the transducer, the conductivity of the copper in the coil, the permeability of the ferromagnetic material, the damping factor of the entire system and the spring constant. A matched simulation was obtained simulating the OMT with the correct parameter setting. The matched simulation was then run through a series of different air gaps in case 4 providing a minimal air gap before saturation. Simulations shows that permeability does not significantly affect the force output of the OMT, while the magnetization vector does affect the force output and saturation of the material. The saturation can be managed by for instance manually increase the air gap until desired force output has been reached.

The developed simulation model is deemed to provide sufficient results when compared to reference measurements. Hence, simulations can be used advantageously when testing and developing OMT, and more generally BAHS. Some optimization investigation has been performed that gives examples on how a simulation environment can be used to develop and optimize the OMT. The simulation can also replace measurements that are difficult to perform in real life, such as how the electromagnetic flux is distributed in the model.

Acknowledgements

We would like to extend our thanks to our examiner at Chalmers, Sabine Reinfeldt for the support and guidance given to us, but also for a great communication throughout the work. We would like to say thank you to our supervisor Tomas Johansson at Oticon Medical, for sticking with us and patiently answering all our questions and for helping us with the entirety of the project. We would like to thank Erik Holgersson at Oticon Medical for giving us a chance to do this master's thesis and for supporting us through it. Other than that we would like to thank Matthias Carlsson and Willhelm Helgesson Råberg for helping to answer our questions and to the rest of Oticon Medical for having us. Thank you also to professor Bo Håkansson for being a great reference and for answering our questions. Thank you also to Björn Bragée and Linus Andersson at COMSOL Multiphysics for helping us with the simulations and for being a great support.

Last, but not least, we would like to thank our family and friends for the unconditional love and support given to us during the entirety of the thesis. Without you it would not be possible och ni vet att vi älskar er.

Danny Messinger and Alexander Vannas, Gothenburg, June 2020

Abbreviations

Air Conduction (AC)
Balanced Electromagnetic Separation Transducer (BEST)
Bone Anchored Hearing System (BAHS)
Bone Conduction(BC)
Decibel (dB)
Finite Element Method (FEM)
Magnetic flux (Φ)
Magnetic flux density ($\boldsymbol{B}$)
Magnetic flux intensity ($\boldsymbol{H}$)
Magnetization vector ($\boldsymbol{M}$
Ordinary differntial equation (ODE)
Oticon Medical Transducer (OMT)
Permeability (μ)
Relative permeability (μ_r)

Contents

List of Figures

List of Tables

1

Introduction

Hearing loss, which means partial or complete inability to hear, is a problem estimated to affect around 466 million people around the world and the projection over time is growing [1]. It is a condition which can occur due to genetics, environment, age or disease/trauma. The severity and extent of the condition is based on the location of the impairment in the ear [2]. Hearing loss can be divided into different categories where the most important are conductive hearing loss, sensorineural hearing loss and mixed hearing loss [3].

Conductive hearing loss occurs when there is a problem transferring sound waves along the pathway of the outer ear, tympanic membrane and middle ear [4]. If a sensorineural hearing impairment is present, the problem lies with the inner ear, the sensory organ such as the cochlea and associated structures, or the vestibulocochlear nerve [4]. A mix of both conductive hearing loss and sensorineural hearing loss is defined as mixed hearing loss.

One way to facilitate conductive and mixed hearing loss is to use a bone conduction (BC) device. A BC hearing device redirects the sound through the skull bone, via vibrations, into the inner ear [5]. The vibrations sets up sound waves into the inner ear, which stimulates the hair cells in the cochlea and directly stimulates the cochlea via the vibrations. By stimulating the hair cells, the auditory nerve is excited which creates a nerve impulse that the auditory cortex in the temporal lobe can interpret [5]. One problem with some BC devices is the attenuation caused by the skin, where a solution is to use a bone anchored hearing system (BAHS). These systems consist of two parts; a titanium bone implant and an external sound processor that is attached to the titanium bone implant via an abutment [5]. The external sound processor, containing the microphones, picks up sounds and converts them into vibrations. The vibrations are then transferred to the embedded implants. The implants vibrates the surrounding bone which further transfers the soundwaves to the skull bone. One BAHS which can be used is the Ponto system from Oticon Medical [6].

BAHS is an essential tool to improve the quality of life for people suffering from partial conductive and mixed hearing loss, to complete conductive hearing loss [6]. The aim for these devices is to maximize the potential gain, whilst minimizing the design of the aid to make sure it is less of a burden to the wearer. This can be done with rigorous testing and model building, which requires a lot of resources. In order to decrease these resources, a simulation environment can be built where an initial testing phase can begin. The virtual environment can also be used to optimize the already existing products, due to the ease of changing different parameters of the BAHS.

1.1 Aim

The aim of this thesis was to create a simulation environment, using COMSOL Multiphysics, for an Oticon Medical Transducer (OMT). The study focused on the magnetic flux in the OMT, which is an electromagnetic transducer, and the force output that is generated from the system. The aim was also to present some optimization of the OMT in regards to saturation and material properties extracted from the simulations.

1.2 Objectives

To be able to test the possibility to create a simulation environment, the simulation was divided into different sub-objectives. The first sub-objective was to model the electromagnetic coil and the permanent magnet, in an effort to make it as close to reality as possible. The next step is to model the electromagnetic system in a stationary case (DC). Then a full simulation using all the parts of the transducer, AC was implemented in a dynamic case.

The simulation was used to answer questions regarding the magnetic flux of the system, as well as the resulting force output given from the magnetic force. Through the simulation platform the saturation of the ferromagnetic material was also investigated in regards to different air gaps in the OMT, the permeability of copper and the magnetization vector used for the permanent magnet.

Some basic real life testing was conducted on the OMT to be able to verify the results obtained.

After the verification the last step was to create simulation striving to optimize the OMT. This was done to further develop the already existing OMT and to learn how an optimization process can be performed in the field of biomedical engineering.

1.3 Limitations

There are many different parts of a BAHS, but the simulations performed in this thesis are limited to the electromagnetic transducer. The reason is that the scope would be too large if all parts were simulated, analyzed and optimized.

Since the thesis is in collaboration with Oticon Medical AB, the transducer examined is from Oticon Medical AB. Some variation might occur if the thesis would have been conducted on other transducers.

The simulation software used will be COMSOL. This is due to previous knowledge with the software as well as student license provided by Chalmers University of Technology. However, there might be a more suitable software for the application that will not be considered in this project, although the industry standard ANSYS was initially considered as an option.

In order to create a simulation environment, some physical assumptions and approximations is needed. Example of such approximation is that the permanent magnet is homogeneous, which is expected to have little to no impact on the results, while the computational cost is significantly decreased. These kinds of approximations are necessary for the simulation to be a sufficient tool, but will cause some conflicts with the real life product. Another example of a needed simplification is that the motion of the spring only is considered to be vertical. This means that the spring does not have any twisting motion which occurs in a real life example.

There are several ways to simulate an electromechanical model using COMSOL Multiphysics. This thesis is focused on using an ordinary differential equation (ODE) developed to describe the system. However, it should be stated that a more complex model can be developed by the use of multiphysics which can combine mechanics with electromagnetism. The reason for a less complex model to be developed is to save computational cost, while still providing sufficient results.

2

Theory

The theory section presents the theoretical background needed to create and understand the simulations. It will be divided into an audiology, an electromagnetic and a mechanics part. The audiology section describes the basics of human hearing as well as the fundamentals of BC hearing and BC devices. The electromagnetic section describes the underlying physics of the electromagnetics in the simulation, more specifically the behavior of the electromagnetic coil and the interplay of the coil and the permanent magnet. The mechanics section describes the underlying physics for the mechanical forces which are generated by the magnetic field.

2.1 Audiology

Hearing is a vital sense for humans, since it provides us with the ability to identify and recognize objects in the world and to communicate. Sound is created when objects vibrate, which produces a variation in pressure [7]. Sound waves can be described mathematically either in the time domain, as sequences of pressure changes or in the frequency domain as a spectrum of tonal components [7].

The human auditory range is between $20Hz$ and $20000Hz$. However, this is a hearing range only a specific few has, and in general the human speech spectrum is classified as between $200 - 8000Hz$ [7]. In this range there is an important speech spectrum where humans are sensitive and where it is possible to discriminate about one decibel (dB) in sound level and about 0.5% change in tonal frequency [7].

2.1.1 Anatomy of the ear

The anatomy of the ear is generally divided into three parts: outer, middle and inner ear. The outer ear is made of a ridged cartillage covered by skin and its main purpose is to collect sound waves and transfer them inwards. The outermost part of the outer ear is called the auricle and helps collect soundwaves, which are then transferred through the auditory canal to the tympanic membrane. The tympanic membrane, also called the eardrum, marks the end of the outer ear and start of the middle ear. The tympanic membrane is a flexible partition that can be vibrated by sound waves, which enables the sound waves to be transferred to the attached bones in the middle ear [8]. A schematic over the anatomy of the ear can be seen in Figure 2.1.

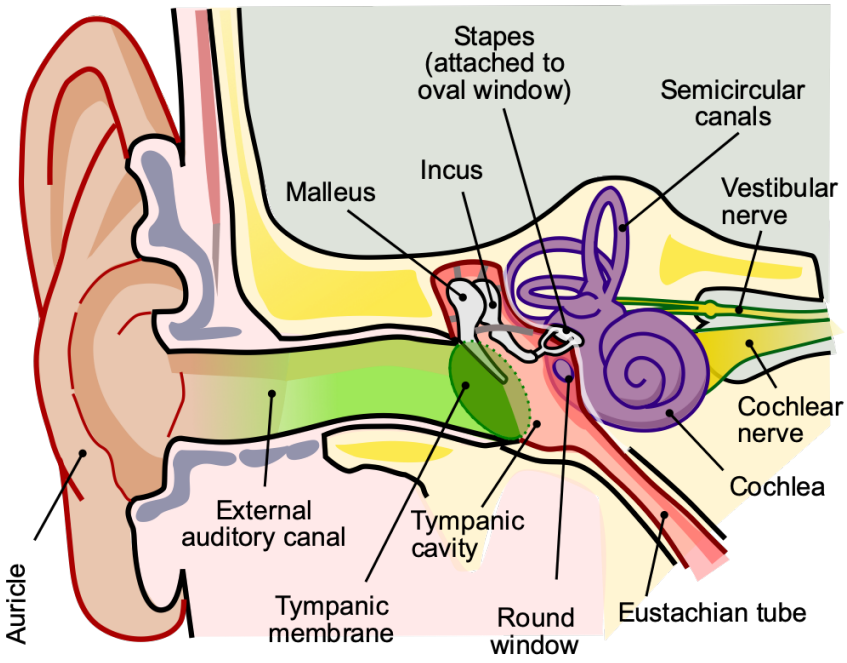

Figure 2.1: A schematic showing the anatomy of the ear. Image taken from [9]

The middle ear is an air filled cavity stretching from the tympanic membrane to the oval window and its primary function is to transfer acoustic energy from compression waves in the air to the inner ear. The middle ear includes the ossicular chain consisting of three bones, Malleus, Incus and Stapes. These transfer the vibrations from the tympanic membrane to the cochlear fluids and membranes of the inner ear [8].

The inner ear consists of the bony labyrinth, which comprises the vestibule, the semicircular canals and the cochlea. The main responsibility of the inner ear is sound detection, performed by the cochlea, and balance, which the vestibular system is dedicated to. The cochlea is a spiral shaped bone structure that has a conical chamber composed of three channels: the scala vestibuli, scala tympani and the cochlear duct. Scala vestibuli and scala tympani are parts of the bony labyrinth making them filled with perilymph fluid although completely separated from each other except at the apex of the cochlea. The vestibular membrane can be found between scala vestibuli and the cochlear duct, while the basilar membrane can be found between scala tympani and the cochlear duct. Supporting cells and hair cells can be found on the basilar membrane, where they are referred to as the spiral organ. The hair cells acts like the receptor for auditory sensations. Motor and sensory neurons synapses are formed from the hair cells created in the cochlear branch of the vestibulocochlear nerve [10].

2.1.2 Hearing Physiology

Hearing can be divided into two blocks, where there are two type of hearing happening simultaneously. There is air conduction (AC) hearing and BC hearing. AC is what one would like to call the conventional way of hearing, where sound waves travel through the different parts of the ear as described in section 2.1.1. The sound is made up of sound waves entering the ear canal [11].

BC hearing is a complement to conventional AC hearing. This is used simultaneously as AC hearing, and for most surrounding sounds, the BC hearing component is negligible in comparison. However, in the case of vocalization, the produced sound waves are transported in two directions: The voice is emitted and transported through the air to the outer ear and then takes the regular AC route, or through internal tissues. This can be shown schematically in Figure 2.2. BC hearing generally has a lower frequency which is the reason to why one's own voice sounds different on recordings [12].

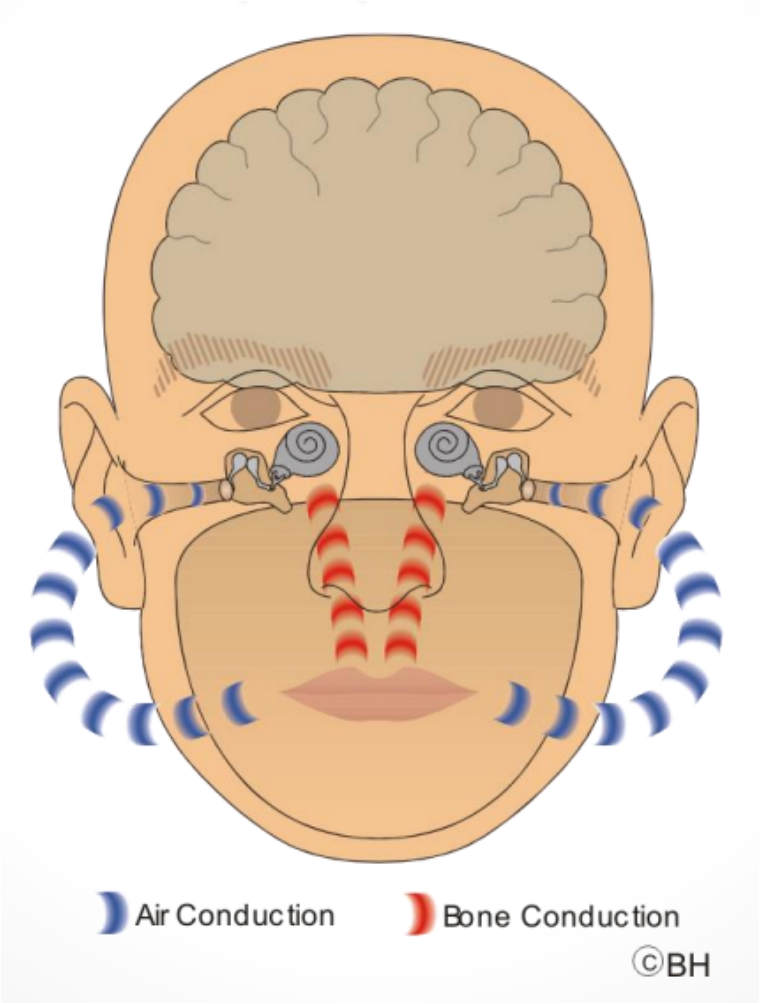

Figure 2.2: How sound is transported through both AC and BC. Image is taken from Sabine Reinfeldt's thesis for the degree of Doctor of Philosophy and is used with consent [12].

Hearing impairments is defined as partial or complete inability to hear. It can occur due to many reasons such as genetics, aging or exposure to noise and can occur in one or both ears [7]. Hearing loss can be categorized into ranges depending on how attenuated the hearing capability is. Slight hearing loss means $16-25dB$ hearing loss, mild $26-40dB$, moderate $41-55dB$, moderately severe $56-70dB$, severe $71-90dB$ and profound greater than $90dB$ [7]. There are three major types of hearing loss: conductive, sensorineural and mixed. Conductive hearing loss occurs when there is a problem transferring sound waves along the pathway of the outer ear, tympanic membrane or middle ear [4]. If a sensorineural hearing impairment is present, the problem lies with the inner ear, the sensory organ such as the cochlea and associated structures, or the vestibulocochlear nerve [13]. A mix of

both conductive hearing loss and sensorineural hearing loss is defined as mixed hearing loss. A person without sensorineural hearing on one or both ears is diagnosed as uni- or bilaterally deaf and complete deafness on one ear can also be determined as single sided deafness [11].

2.2 Bone Conduction Hearing Systems

In order to facilitate conductive and mixed hearing loss, it is possible to use a BC hearing system. The BC hearing system redirects the sound through the skull bone since the outer or middle ear cannot be used as intended. The sound is vibrating the skull bone into the inner ear creating sound waves that directly stimulates the cochlea [5]. Several BC hearing systems exists and they can mainly be categorized into skin drive and direct drive systems [14]. Conventional BC hearing systems, which belongs to the skin-drive systems, consists of a vibrating transducer that is pressed against the skin using a soft band or a steel spring arrangement. The skin-drive systems transfer external vibrations via the intact skin to the skull bone [15]. Since the skin is intact, attenuation of the vibrations caused by the skin will occur resulting in lower sound levels reaching the cochlea. A solution to this is to introduce the direct drive BC hearing system, where the vibrations are directly transferred to the skull bone [5]. This can be done in two ways, either percutaneously or transcutaneously. The active transcutaneous BC hearing system consists of an implanted transducer into the skull bone where the sound is passing through the intact skin wirelessly [15]. The percutaneous BC hearing system is when the vibrating transducer is attached to a titanium screw that penetrates the skin where it is anchored in the skull bone, which is called a BAHS [12]. The external sound processor picks up sounds and then converts them into vibrations [6]. The vibrations are then transferred to the embedded implants. The implants vibrates the surrounding bone which further transfers the soundwaves to the cochlea. Examples on BAHS is the Baha® from Cochlear [16] and the Ponto system from Oticon Medical AB [6]. There are also BAHS consisting of other transducers, such as the balanced electromagnetic separation transducer (BEST) [17].

2.3 Electromagnetism

The study of the effects of electric charges at rest and in motion is called electromagnetism [18]. Electromagnetism has four fundamental vector quantities, seen in Table 2.1. The factor between the electric field intensity, $\boldsymbol{E}$, and the electric field density, $\boldsymbol{D}$, is a dielectric constant called permittivity, ϵ, that is dependent on the permittivity of free space, ϵ_0, and the material dependent relative permittivity, ϵ_r, see equation 2.1. Similarly the magnetic field density, $\boldsymbol{B}$, and the magnetic field intensity, $\boldsymbol{H}$, are related via the permeability, μ, that consist of the permeability of free space, μ_0 and the material dependent permeability, μ_r, see equation 2.2 [19].

$$\boldsymbol{E} = \frac{\boldsymbol{D}}{\epsilon} = \frac{\boldsymbol{D}}{\epsilon_0 \epsilon_r} \tag{2.1}$$

$$\boldsymbol{H} = \frac{\boldsymbol{B}}{\mu} = \frac{\boldsymbol{B}}{\mu_0 \mu_r} \tag{2.2}$$

Table 2.1: The fundamental vector quantities of electromagnetics and the SI units

Field quantity	Unit
Electric field intensity, $\boldsymbol{E}$	$[V/m]$
Electric flux density, $\boldsymbol{D}$,	$[C/m^2]$
Magnetic flux intensity, $\boldsymbol{H}$	$[A/m]$
Magnetic flux density, $\boldsymbol{B}$	$[T]$

Whenever a charge is in motion in a magnetic field, it will experience a force called the magnetic force, F_m. The magnetic force is proportional to a charge, q, and in the perpendicular direction of the velocity, $\boldsymbol{v}$, of the charge [18, p.225]. In order to decide the attributes of the magnetic force, the magnetic flux density, $\boldsymbol{B}$, needs to be introduced. The magnetic flux density can be described by Ampère's circuital law stating that the total permeability, μ, times the total current flowing through a bounded surface is equal to the circulation of the magnetic flux density, see equation 2.3 [p.227][18].

$$\oint_C \boldsymbol{B} \cdot d\ell = \mu I \tag{2.3}$$

Since $\boldsymbol{B}$ is related to $\boldsymbol{H}$ via the total permeability, equation 2.2, Ampère's circuital law can accordingly be described by equation 2.4, stating that the circulation of $\boldsymbol{H}$, inside a closed path is equal to the currents flowing through the bounded surface.

$$\oint_C \boldsymbol{H} \cdot d\ell = I \tag{2.4}$$

The magnetic force, F_m, can be described using equation 2.5, where q is the charge, $\boldsymbol{v}$ is the velocity of the charge and $\boldsymbol{B}$ is the magnetic flux density [18, p.226].

$$F_m = q\boldsymbol{v} \times \boldsymbol{B} \ \ [N] \tag{2.5}$$

In order to express the total electromagnetic force, the electric force is added to the magnetic force, which provides the Lorentz´s force equation, see equation 2.6, where q is the charge, $\boldsymbol{E}$ is the electric field intensity, $\boldsymbol{v}$ is the velocity of the charge and $\boldsymbol{B}$ is the magnetic flux density [20].

$$F = q(\boldsymbol{E} + \boldsymbol{v} \times \boldsymbol{B}) \tag{2.6}$$

The magnetic flux, Φ can be defined from $\boldsymbol{B}$ by integrating over the surface, see equation 2.7 [18, p.234]. This is due to that $\boldsymbol{B}$ corresponds to the amount of Φ passing through a perpendicular area [21].

$$\Phi = \int_S \boldsymbol{B} \cdot ds \tag{2.7}$$

Atoms consists of positive and negative charges. The electrons that carries the negative charge is orbiting around the nucleus of the atom which provides small circulating currents. These currents forms microscopic dipoles that, in most materials, are randomly oriented in the absence of a magnetic field. If the direction of the magnetic dipoles are aligned, they form so called domains and if an external magnetic field is applied, the magnetic dipoles domains would align with the external field. The magnetic dipole moment, m, is defined as the strength and the orientation of the magnetic moment in each individual atom. A magnetization vector, $\boldsymbol{M}$, is defined as the magnetic dipole moment per unit volume, see equation 2.8 [18, p.244].

$$\boldsymbol{M} = \frac{dm}{dV} \tag{2.8}$$

The introduction of an external magnetic field causes $\boldsymbol{H}$ to also be dependent on $\boldsymbol{M}$, together with the earlier defined permeability of the material and $\boldsymbol{B}$, see equation 2.9.

$$\boldsymbol{H} = \frac{\boldsymbol{B}}{\mu} - \boldsymbol{M} \tag{2.9}$$

Materials can be divided into subgroups, depending on their magnetic behavior. If the relative permeability, μ_r, of the material is a small positive number, the material is categorized as paramagnetic. Paramagnetic materials do not imply an increase in Φ when exposed to an external magnetic field. The paramagnetic materials are temperature dependent, where the paramagnetic behavior material is more vigorous in lower temperature. An example of a paramagnetic material is tungsten, where μ_r is close to one [18, p. 258].

Another subgroup of materials in regards to the magnetic behavior is ferromagnetic material. Ferromagnetic materials have $\mu_r >> 1$. This property makes the material partially or fully magnetized. A material is partially magnetized when some magnetic dipole domains within the material are aligned and fully magnetized when all the magnetized domains are aligned. If the magnetic dipole moments are difficult deranged, an external magnetic force would not change the domain alignment and therefore be permanently magnetized [18, p. 258].

A common way to analyze ferromagnetic materials is by the use of the $\boldsymbol{B} - \boldsymbol{H}$ plane. The number of aligned magnetic dipoles will increase when the ferromagnetic material is exposed to an external magnetic field, increasing the volume of the magnetic domains. Due to this, $\boldsymbol{B}$ is increased until all domains are aligned. When all domains are aligned and the external magnetic field is further increased, the field density will stay on a steady level. This phenomena is called saturation of the material and implies that the maximum flux density, for the material, has been reached [18, p. 257].

A coil is a winded metal that can be enclosed with the use of a bobbin. When the coil is induced with a current, it will work as an electromagnet. This implies that the winded metal need to have high conductivity to allow the current to pass through the coil. The conductivity is defined as the inverse of the resistance in the material. The magnetic flux passing through the coil can be described as the flux passing through each circulation of winding. The flux linkage, $\Lambda = \Phi \cdot N$, is therefore introduced to link the magnetic flux to

the number of turns, N, in the coil. The inductance of the coil can then be described by the flux linkage and the induced current according to equation 2.10 [18, p. 267].

$$L = \frac{\Lambda}{I} \tag{2.10}$$

The electromagnetic force can be expressed in terms of the magnetic flux according to equation 2.11. If a ferromagnetic material is placed on a small distance from an electromagnet, with an air gap defining the difference, then the electromagnetic force on the distant ferromagnetic material will experience an electromagnetic force in accordance with equation 2.11. The equation describes the electromagnetic force, F, in the air gap, μ_0 is the permeability in free space and S is the cross-sectional area of the core [22]. The negative sign indicates that an increase in the electromagnetic force will decrease the length of the air gap. This knowledge can be used to decide an air gap for a given electromagnetic force.

$$F = -\frac{\Phi_{tot}^2}{\mu_0 S} \tag{2.11}$$

When introducing a permanent magnent to the electromagnet and the medium is considered linear, then the total magnetic flux, $\Phi_{tot} = \Phi_s + \Phi_d$, where Φ_s is the static magnetic flux and Φ_d is the dynamic magnetic flux. Φ_s is the flux generated from the permanent magnet and Φ_d is the alternating flux created by the varying current induced in the coil. Φ_d^2 can be viewed as distortion and $\Phi_s >> \Phi_d$ [22]. Since equation 2.11 shows that the electromagnetic force is proportional to Φ_{tot}^2 through the surface perpendicular to the air gap, it can be simplified to equation 2.12. The oscillating current, causing the dynamic flux, will enable the system to vibrate due to $2\Phi_s\Phi_d$ seen in the equation.

$$F \propto \Phi_{tot}^2 \longrightarrow F \propto \Phi_s^2 + 2\Phi_s\Phi_d + \Phi_d^2 \tag{2.12}$$

2.4 Mechanics

The transducer is driven by a magnetic force, which will be the driving force of the mechanical system. However, the mechanical part of the transducer is characterized by the spring force. This section provides basic information regarding the dominating mechanical force affecting the transducer and how a system in harmonic oscillation behaves.

The simplest example of the spring force is Hooke's law which can be seen in equation 2.13 [23]. The equation shows that the spring force in a stationary state is defined as the displacement, x, of an object connected to a spring, indicating how much a spring has stretched, multiplied by the spring constant, k, which defines the stiffness of the spring [23].

$$F = kx[N] \tag{2.13}$$

The stationary case of Hooke's law can be used to determine initial states of the system. However, to use Hooke's law in a more realistic scenario, the spring force can instead be

modeled as in equation 2.14 [23]. In this case the spring force is modeled as a differential equation where the force is equal the sum of three different terms, that are dependent on time. The first term is the second derivative of the displacement multiplied with the mass attached to the spring. The second term is a damping ratio ξ multiplied by the first derivative of the displacement and the last term is the original stationary case [23]. The damping ratio is defined with equation 2.15 which is a ratio of the actual damping d divided by the critical damping [24]. The critical damping is derived from the natural frequency, which is the frequency where the system resonates. The expression for this can be seen in equation 2.16, where the natural frequency is the square root of the spring constant divided by the mass of the moving object [24]. The system described by these equations is a driven harmonic oscillator, also called a parametric oscillator. The most important property for the system to work is that the damping ratio is between one and zero. Otherwise the system is over-damped, which will cause it to not oscillate [24].

$$F(t) = mx'' + 2\xi\omega_n x' + kx \tag{2.14}$$

$$\xi = \frac{d}{2m\sqrt{\frac{k}{m}}} \tag{2.15}$$

$$\omega_n = \sqrt{\frac{k}{m}} \longrightarrow f_n = \frac{1}{2\pi}\sqrt{\frac{k}{m}} \tag{2.16}$$

To describe the system in the frequency domain, a Fourier transform of the differential equation can be made, which can be seen in equation 2.17. The basics of the Fourier transform is that each differential of the previous equation gives a frequency dependent term.

$$F(j\omega) = -m\omega^2 X(j\omega) + 2\xi\omega_n j\omega X(j\omega) + kX(j\omega) \tag{2.17}$$

2.5 Transducer

In order for the BAHS to transfer the vibrations into the abutment, the titanium screw and on to the skull bone a transducer is needed. The transducer consists mainly of an electromagnetic part and a mechanical part. The electromagnetic part can be seen in Figure 2.3, where the black part is the bobbin surrounding the orange coil. On top of the bobbin is the permanent magnet, which creates the static magnetic field. The green part is the vibrator plate that is attached to the abutment that can be mounted to the titanium screw in the skull bone. Section 2.3 is implying that the electromagnetic force from the permanent magnet and the coil wants to attract the vibrator plate, that consists of a ferromagnetic material. The electromagnetic force will increase as the air gap separating the vibrator plate gets smaller.

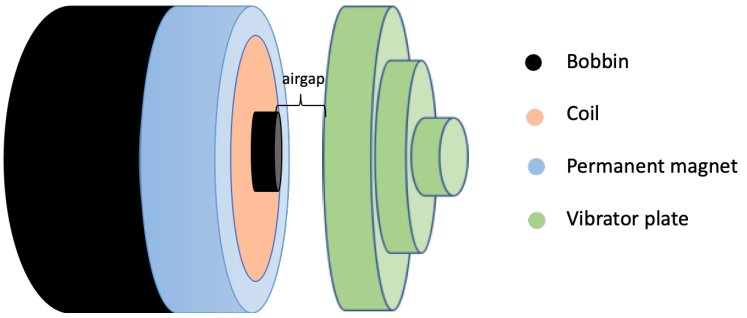

Figure 2.3: Overview of the electromagnetic parts in an OMT transducer, where the black part correspond to the bobbin, the blue to the permanent magnet, the orange to the coil and the green to the vibrator plate.

A spring is attached to the vibrator plate in order to counteract the electromagnetic force exerted on the vibrator plate. In order to create the spring mass system a tungsten frame is added connecting the bobbin to the spring. Since tungsten is a paramagnetic material it is not expected to be affected by the electromagnetic field. The tungsten frame, bobbin, coil and permanent magnet are collectively called the moving mass. The moving mass is moving in relation to the vibrator plate, since the vibrator plate is attached to the skull bone and can therefore be seen as fixed. A 2D representation of the different parts of the transducer can be seen in Figure 2.4.

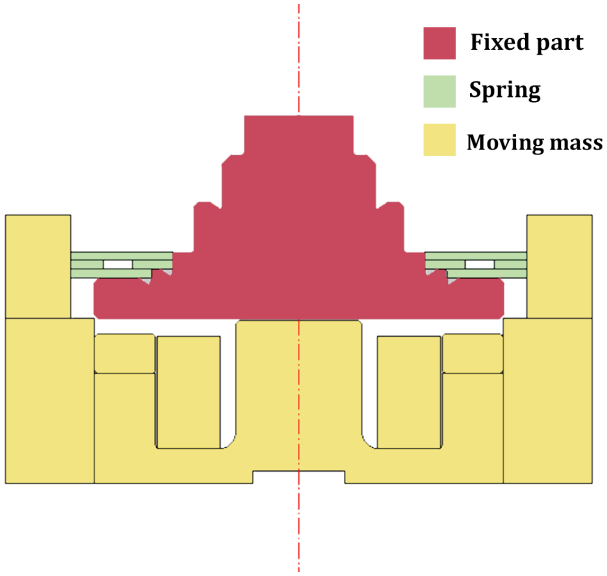

Figure 2.4: A cross section of the transducer, where different parts are highlighted depending on if they are movable or not. Red is the fixed part, yellow is the moving mass and green is the spring.

The transducer can thus be described as a spring mass system, see Figure 2.5a, with an electromagnetic motor, see Figure 2.5b. To describe this system, equations from sections 2.3 and 2.4 can be used. The mechanical part of the spring mass system can be described by equation 2.14, where the system is a damped driven system with an external force applied. The driving force is explained in equation 2.12, where the force is related to the magnetic flux. The difference from the regular equation is that the magnetic and mechanical forces oscillates around an equilibrium point, instead of canceling each other.

A magnetic force from the permanent magnet wants to collapse the system while the transducer spring is keeping the small air gap from collapsing. This means that to use equation 2.12, a linearization around the working point is necessary.

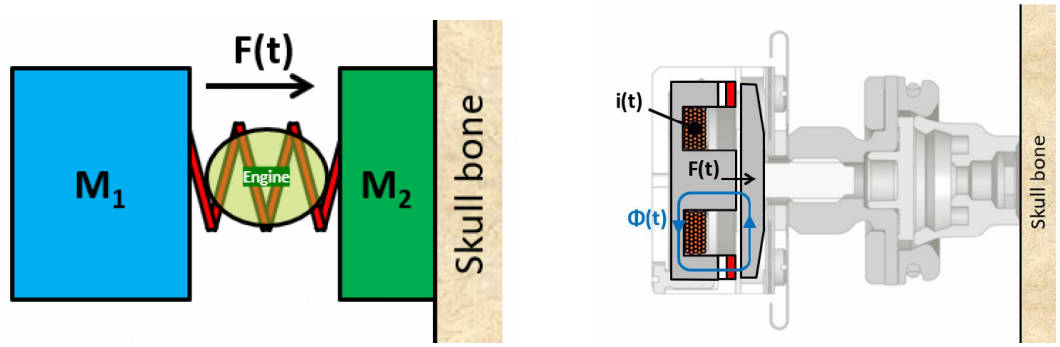

(a) (b)

Figure 2.5: The proposed spring-mass system which is used to simplify a hearing aid system in (a), and of the motor which generates the vibrations (b). Both images are used with courtesy of Oticon Medical [25]

In order to calculate the displacement caused by the force it is possible to use Newton's second law, see equation 2.18, where the displacement from the equilibrium point is called s and m is the mass of the moving mass [26]. Since the induced current is sinusoidal the displacement can be described from equation 2.19. Equation 2.18 and 2.19 combined gives equation 2.20 [23].

$$F = m\frac{d^2s}{dt^2} \tag{2.18}$$

$$s(t) = A\sin(\omega t) \tag{2.19}$$

$$F = m\frac{d^2s}{dt^2} = m\frac{d^2sin(\omega t)}{dt^2} = -m\omega^2 s \tag{2.20}$$

When describing the total force output of the transducer a combination between the electromagnetic force, see equation 2.6, the spring force, see equation 2.17 and equation 2.20 can be combined to provide the ODE in equation 2.21, where F_m is the electromagnetic force, k is the spring constant, s is the displacement, d is the damping factor, ω is the angular frequency and m is the mass of the moving mass.

$$F_{tot} = -F_m + ks + jd\omega s - m\omega^2 s \tag{2.21}$$

2.6 Finite Element Method

The Finite element method (FEM) is one of the most widely used methods for solving mathematical models and engineering models and can be used to solve electromagnetic

problems [27]. The FEM is a numerical method which solves partial differential equations. To solve the differential equations the FEM divides a system into smaller parts which can be solved individually. The smaller parts are called finite elements and is created by meshing, which is dividing the model into grids [27]. By implementing a mesh, the FEM discretizes in space creating space variables (x,y,z). By discretisizing the model, the FEM creates a system of smaller algebraic equations, which can be solved locally by approximating the unknown function over the domain. When the boundary equations have been solved locally, they can be assembled into a larger system of equations modelling the entire system [27]. To solve the smaller algebraic equations a variation of calculus methods can be used to approximate a solution by minimizing an error function [27].

One calculus method to approximate a solution by minimizing an error function is the Newton method. The equation for the Newton method can be seen in equation 2.22 [28]. The idea of the algorithm is to find a better estimate, $f(x_+, y)$, by analyzing the function of an eligible guess of the system, f(x,y), where x is the initial guess. Equation 2.22 is a first order Taylor approximation of $f(x, y)$ and the equation can be described in its affine form with equation 2.23. The method is iterative and repeats until $f(x, y) = 0$, or at least until it is below the specified tolerance [28].

$$f(x_+, y) \approx f(x, y) + \frac{\partial f(x, y}{\partial x}(x_+ - x) + \mathcal{O}(||x_+ - x||^2) \tag{2.22}$$

$$x_+ = x - \frac{\partial f(x)^{-1}}{\partial x} \tag{2.23}$$

The FEM simulation can be created using different software application. In this thesis two different software was initially considered. These are called ANSYS and COMSOL Multiphysics. The chosen software is COMSOL Multiphysics due to previous experience regarding electromagnetic simulations using COMSOL Multiphysics together with a proposal from Oticon Medical to use the specific software. COMSOL Multiphysics is a simulation software that enables multiphysics combinations to investigate a system [29].

COSMOL uses FEM to discretize the model by meshing with tetrahedrals. To compute the partial differential equations, COMSOL uses a version of the Netwon method, that is called damped Newton method [29].The difference between the damped Newton Method and the classical Newton method is that the damped ensures that a damping is in place on the Newton step. This ensures that a sufficiently small step is taken, which will help convergence [30].

3

Method

To be able to conduct a simulation with a software such as COMSOL, there are some general steps that are needed to be done. Firstly, the correct preset must be chosen. This includes which type of geometry being simulated, for example a 3D-model or a 2D-axisymetric model, and also which type of study is needed. In order to simulate the model several studies can be chosen. The study is dependent on how the model should be evaluated. In this thesis a stationary analysis, a time dependent analysis and a frequency domain analysis are performed.

The next general step was to build the geometry and then choosing the materials for each component. The models for this thesis can be seen in Figure 3.1, where Figure 3.1a shows the model in 2D where it is a cross section of the 3D model, and Figure 3.1b shows the model in 3D. The reason behind having both a 2D and a 3D model is that the simulations are done in both 2D and 3D. As can be seen in the images the models are color coded to show the different parts of the transducer, explained in section 2.5. The material used to model the vibrator plate and the bobbin was a cobalt-iron alloy, which is a ferromagnetic material. Copper was used as material for the coil, steel was used to model the spring and tungsten was used for the frame, where all materials chosen are listed in Table 3.1.

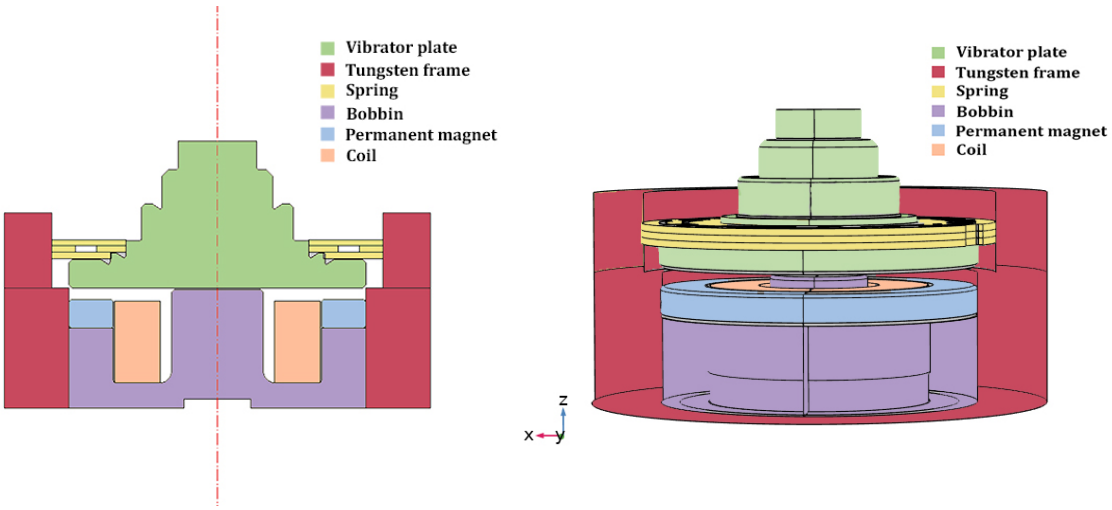

(a) 2D model of transducer

(b) 3D model of transducer

Figure 3.1: The different parts of the transducer, in a 2D and 3D model.

Table 3.1: The materials used for the different parts of the OMT.

Material	**Part in model**
Cobalt-iron alloy	Vibrator plate and bobbin
Copper	Coil
Steel	Spring
Tungsten	Tungsten frame

The next step for setting up a simulation was defining the physics of the simulation, including boundary conditions for the different domains. In case of a multi-physics problem, which was the case for the electromechanical simulation in this project, some domains can have multiple boundary conditions. The last step before the simulation was to create the mesh of the system. COMSOL uses a physics defined mesh, which changes its size depending on the complexity of a given part of a model. For example a corner will need smaller elements of the mesh, since it is not a smooth surface. However, the mesh can also be refined manually by applying different sizes of the mesh elements to different areas. This was important since the damped Newton method can't converge if the mesh element is too rough. When all of this was done, the model can be assembled to complete a simulation.

The conducted simulation was divided into four cases where each case increases the complexity in the model, see Figure 3.2. In the first case, the electromagnetic and mechanical components were individually tested and evaluated. The evaluation was compared with measured performance of an OMT, to have the correct characterization of the individual parts. The second case described how the individual parts are assembled and evaluated using a static case corresponding to the application of a DC voltage, with no movement in the model. The third case was to implement a frequency domain and time domain analysis, where the model can move with a range of frequencies or period of time. The fourth and final case provided simulations in which some parameters were changed, to provide information regarding optimization of the OMT.

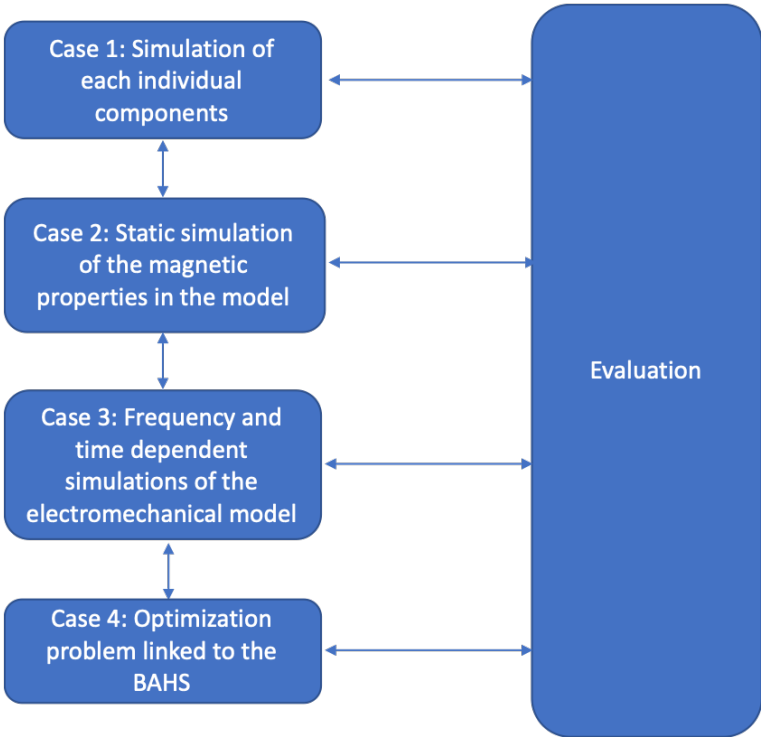

Figure 3.2: Flow chart showing the working process of the conducted cases in the thesis.

3.1 Case 1

The first simulation case was dedicated to individually test the functionality of the components that mainly affects the results. This included the permanent magnet, the coil and the spring.

The permanent magnet creates a static magnetic field and the coil is creating the variations of the dynamic magnetic flux related to equation 2.7. The spring is counteracting the static force to create an equilibrium point where the vibrations are taken place.

In order to simulate the static magnetic flux given from the permanent magnet, the magnetic fields physics was used in COMSOL Multiphysics. The magnetic fields physics option was used to simulate the magnetic field and currents distributions on magnets and coils. In order to define the magnet according to the OMT a magnetization vector was used as the magentization model. The magnetization vector was calculated using an electric dipole moment measured from the permanent magnet of a real transducer. The reason for using this method was to assure the correct magnetization when compared to a real life OMT. The magnetic dipole moment was measured to be $2.7 \mu V scm$, where V is volts, s is seconds and cm is centimeter.

As described in section 2.3, the theoretical magnetic dipole moment is related to $\boldsymbol{H}$ via the magnetization vector. However, the measured magnetic dipole moment is based on $\boldsymbol{B}$. From section 2.3 it is stated that the relation between $\boldsymbol{H}$ and $\boldsymbol{B}$ is the permeability. The magnetization vector was calculated to $6.7849 \cdot 10^5 Am^2$ using this relation and equation 2.8. The calculated magnetization vector is inserted to the simulation to describe the magnetization of the permanent magnet.

The second part of the OMT to be individually tested was the coil. In the magnetic fields physics option, it is possible to add a coil in which several parameters is to be set. The choice of material for the coil was copper. The simulation used data, such as the conductivity and permeability, that are specified within the material. These values can be changed, but are initially set by COMSOL to mimic the real life material properties. The coil was set to be a homogenized multi turn where the coil cross section area was decided together with the number of turns. It was also of importance to define where the coil excitation is taking place. The magnitude of the coil excitation was compared to data gathered by Oticon Medical and typical voltage applied on the coil. The coil was evaluated according to a given resistance from measurements performed, with the help from Oticon Medical, and from drawings.

In order to evaluate the spring, i.e. the mechanical part of the system, the spring constant was simulated. The simulation used Hookes law, equation 2.13, where solid mechanics was used as physics in COMSOL. The spring was fixed, similarly to the OMT in real life, using a fixed constraint in COMSOL. An arbitrary force was then added on the outside of the spring. The spring constant can be calculated using the applied force and the displacement of the spring generated from the simulation, see equation 2.13. The spring was measured in the lab, with the help of Oticon Medical, as a reference for the simulations.

3.2 Case 2

The second study case aimed at investigating the system when assembled, in a stationary environment. To do this, all the individual parts are built within the same geometry in COMSOL. Since a stationary study does not allow any movement in the model, it was unnecessary to model the spring in this case. The spring would inflict a higher computational cost whilst not affecting the results, since no movement can take place. The assembled model can be seen in Figure 3.3. To evaluate the simulations a so called point evaluation was used, where four points was chosen and placed according to Figure 3.3a. As can be seen in the figure, the yellow point is placed on the bottom of the vibrator plate, the orange point on the top of the bobbin tower, the blue point in the middle of the bobbin tower and the purple point in the corner between the coil and bobbin. These points are expected to show the regions where the magnetic flux is of interest.

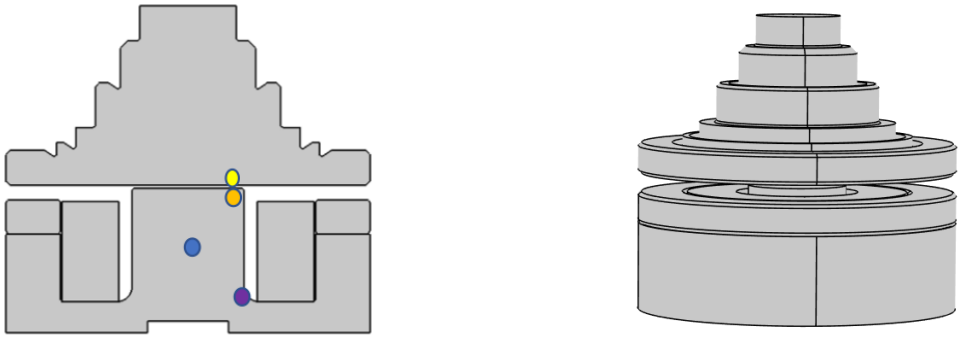

(a) The electromagnetic parts of the transducer in a 2D model

(b) The electromagnetic parts of the transducer in a 3D model

Figure 3.3: The geometries used for case 2 in a 2D and 3D model. Figure 3.3a shows the evaluated points of interest. The yellow point is placed on the bottom of the vibrator plate, the orange point on the top of the bobbin tower, the blue point in the middle of the bobbin tower and the purple point in the corner between the coil and bobbin.

To simulate the static magnetic flux in the entire model, the magnetic fields physics in COMSOL was used. The settings mimic case 1, to be able to compare the results. This includes the magnetization vector for the permanent magnet and the homogenized multi-turn coil. To verify the the strength of the magnetic flux and to ensure that the material parameters are working correctly, the saturation of the ferromagnetic material was simulated. The simulation results were compared with datasheets available for the ferromagnetic material. If the material is saturated, the transmitted force in the air gap is expected to decrease, in compliance with section 2.3. The cobalt-iron alloy used in the vibrator plate and bobbin is saturating at $2.3T$ [31]. The saturation of the material is also something that is simulated using a $\boldsymbol{B} - \boldsymbol{H}$ plane, where different parts of the OMT was analyzed.

3.3 Case 3

The third case investigated the frequency and time dependence of the system. This could be done by combining the magnetic field node with the solid mechanics node, to enable movement of the different components as described in Figure 2.4. Another way of enabling this was by solving the ODE, described in equation 2.21, directly with an ODE node in COMSOL, where the purpose was to solve for the state variable "s", which represents the displacement of the moving mass.

For this assignment the option of solving the ODE was used, due to the fact of it requiring less computational cost, which allowed more powerful simulations. As mentioned in section 2.5 the system could be described as a spring mass system with forced damped

vibrations and one degree of freedom. The force output was calculated from the displacement through equation 2.21.

Figure 3.4 shows the method used for this case. The parameters for the simulation was initially setup by analyzing the previous cases. For example, the spring constant, k, was given from the result analysis from case 1, and the permeability was investigated, among other attributes, in case 2. The next step in the simulation was to perform a stationary analysis. The reason behind this was to evaluate the working point created by the static magnetic flux from the permanent magnet. The stationary analysis evaluated the magnetic force generated from the permanent magnet and calculates how much closer to the moving mass the vibrator plate is pulled, before the system reaches an equilibrium point. The magnetic field from the coil is negated in its entirety due to the use of the linear perturbation operator on the voltage input. The linear perturbation operator states that the voltage input should only be applied in the frequency domain and that the coil works as a small signal model.

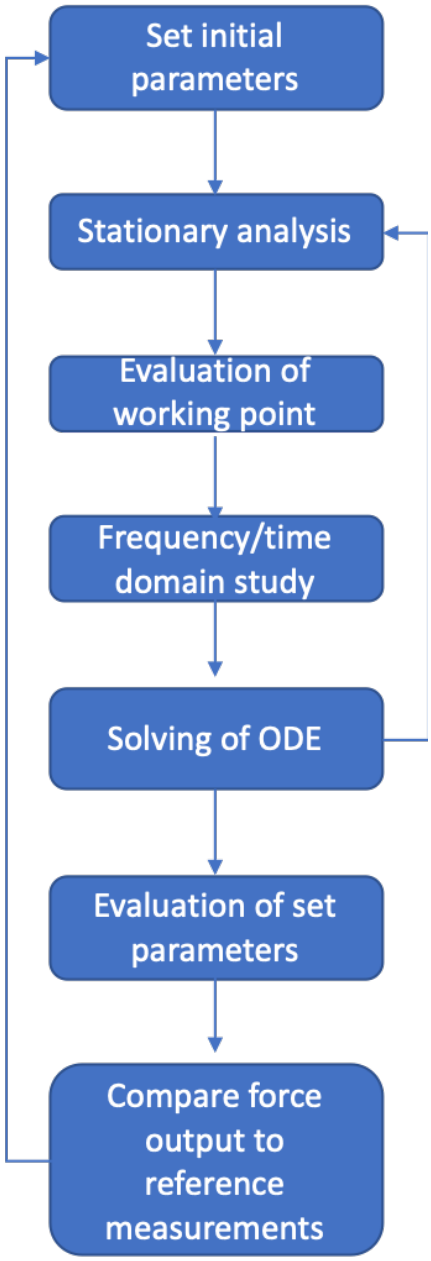

Figure 3.4: The work flow of the simulation in case 3.

After the working point was evaluated and an appropriate air gap had been set, a frequency domain study step was used to investigate the frequency dependence of the system. The frequency domain study step performs a frequency sweep, in this case between $100 - 10000Hz$ with a step size of $10Hz$. The reference frequencies, used by Oticon Medical, are around $400Hz$, around the resonance frequency and around $3000Hz$ [25]. The frequency given from the frequency domain step becomes a variable in the next step in the simulation. The next step of the simulation was the solving of the ODE. In this step the program used the input frequency as a parameter in the differential equation given by equation 2.21 in section 2.5.

In order to verify and validate the results given from the simulations, 10 measurements were performed in the lab at Oticon Medical. The measurement setup includes a Clio fw from Audiomatica, a skull simulator and an OMT. The Clio fw is an electrical and acoustical measurement system and the skull simulator is a fixed mass of $64g$, similar to a human skull bone when exposed to vibrations around $1000Hz$, and converts force output to voltage. In the Clio fw software application an rms voltage was chosen to be applied. A stepped frequency analysis with a range from 10 to 10000 Hz was then chosen to make the measurements as close to the simulations as possible. As stated in the previous section the simulation was running a stationary solver for each

frequency tested. This would result in that no energy from the previous frequencies were transferred to the newly simulated frequency. This means that the measurements needs to be shut down between each frequency in order to obtain the same results. The stepped function is resetting the signal between each frequencies in the measurement, mimicking this property.

Five parameters were considered in order to change the the characteristics of the simulations. These can be found in Table 3.2, where the air gap was expected to affect the entire simulation, the conductivity and the permeability were expected to mainly affect low frequencies, the damping factor and the spring constant was expected to mainly affect the resonance frequency. These parameters could be optimized in order to match simulations to real life testing of the OMT.

Table 3.2: Parameters that can be changed in order to affect the characteristics of the simulation.

Parameters:	Air gap	Conductivity	Permeability	Damping factor	Spring constant

3.4 Case 4

The fourth case is investigating different attributes of the OMT. There are multiple attributes that could be simulated when optimizing a product, where three are considered in this thesis. The first attribute to be tested was how the force output varies with the change of permeability in the material. The second attribute was how the force output varies with different magnetization vectors, as the magnetic dipole moment in the permanent magnet can vary. The third attribute was how the force output changes with different air gaps. The studied attributes can be seen in Table 3.3.

Table 3.3: The three attributes altered to see how they affect the force output.

Studied attributes
Permeability of the cobalt-iron alloy
Magnetization vector of permanent magnet
Different air gaps

Three relative permeabilities was investigated. These were chosen as the minimum permeability, the maximum permeability and the mean of the maximum and minimum permeability. The chosen permeabilties can be seen in Table 3.4. The minimum permeability was 1000 and considered to be the minimum permeability after production of the ferromagnetic material. The maximum permeability was 4500 and considered to be the maximum permeability after production of the ferromagnetic material and the mean between the maximum and minimum permeabilities was 2750. In order to perform the simulations a linear relative permeability model was used. This means that the permeability in the material was was not alternating depending on saturation and the B-H plane. This was a simplification done in order to investigate the impact of fixed permeabilities.

Table 3.4: The different relative permeabilities which were simulated

Relative permeability, μ_r
1000
2750
4500

The magnetization vector was expected to vary between $6.5336 * 10^5 A/m$ and $7.2875 * 10^5 A/m$ after production. Similarly to the permeability, a mean value was calculated from the maximum and minimum magnetization vector to $6.9106 * 10^5 A/m$. A transducer with a weak magnetization vector and a low permeability would need a smaller air gap to get the same force output as a transducer with a strong magnetization vector and high permeability. To simulate the magnetization vector a B-H model was used to decide the permeability of the material. This method is expected to provide information about the saturation of the material when the magnetization vector was altered. The magnetization vectors investigated can be seen in Table 3.5.

Table 3.5: The different magnetization vectors which were simulated

Magnetization vector, $\boldsymbol{M}$ **[A/m]**
$6.5336 \cdot 10^5$
$6.9106 \cdot 10^5$
$7.2875 \cdot 10^5$

When deciding the size of the air gap there was a contradiction making it possible to obtain the minimal possible air gap before saturation. It is stated in section 2.3 that a smaller air gap in the transducer is generating a higher force output, meaning that a small air gap would be preferred. However, it was also stated in section 2.3 that the material can be saturated resulting in a decrease of force output if the air gap is getting too small. A total of twelve different air gaps are simulated in order to find the smallest air gap at which the the material is not saturated. The air gaps tested can be seen in Table 3.6.

Table 3.6: The different air gaps [μm] tested in the simulation, in an effort to optimize the OMT.

131.5	119.6	107.2	94.27	80.34	72.63	64.51	55.45	46.5	37.4	28.3	21.02

4

Result

The result section is divided similarly as the method section, where the results from every case are presented one by one.

4.1 Case 1

The purpose of the first case was to analyze the different parts of significance, by themselves, to certify that they were functioning properly. The parts that had the biggest influence on the results were the coil and permanent magnet for the magnetic field and the spring for the mechanics. The simulation results are presented in a magnetic field section and a mechanics section.

4.1.1 Magnetic Field

To test whether or not the coil of the transducer was working correctly, two parameters were tested: $\boldsymbol{B}$ and the coil resistance. $\boldsymbol{B}$ given from the coil when placed in the magnetic circuit, with a DC voltage of $517mV$, was $0.16T$. This is compared to the total $\boldsymbol{B}$ given from the permanent magnet and the coil, which is $1.9T$. The coil is generating $0.16T$ out of $1.9T$ which corresponds to 8.4% of the total $\boldsymbol{B}$. This is in line with values approximated from Oticon Medical and confirms that the $\Phi_s >> \Phi_d$, see section 2.3.

The measured resistance from the coil is 8.9Ω which also corresponds to the stated resistance in the datasheet. However, the simulated resistance is 7.76Ω. This means there is a difference of 30% in resistance. One possible cause of this could be that a difference in conductivity needs to be added to the simulation. This difference in conductivity might be due to the winding of the copper wire in the coil. The coil is modeled to have the same geometric properties as the real life coil. However, this means COMSOL will try to distribute the number of turns with the input wire radius as tight as possible across the entire geometry. In real life, the coil can never be wound as tightly, and together with that there is an insulation around the copper wire, means a longer wire is needed than in the theoretical case. This is illustrated in Figure 4.1, where Figure 4.1a shows how it is wired in the actual coil and Figure 4.1b shows a simplification of the coil used by COMSOL. This difference means that a longer copper wire is used to create the coil in real life which means that the coil will have a higher resistance. This difference in conduction is compensated by decreasing the conductivity of the material in COMSOL. The scale in Figure 4.1 is excessive and shows a schematic of the distributed copper wires.

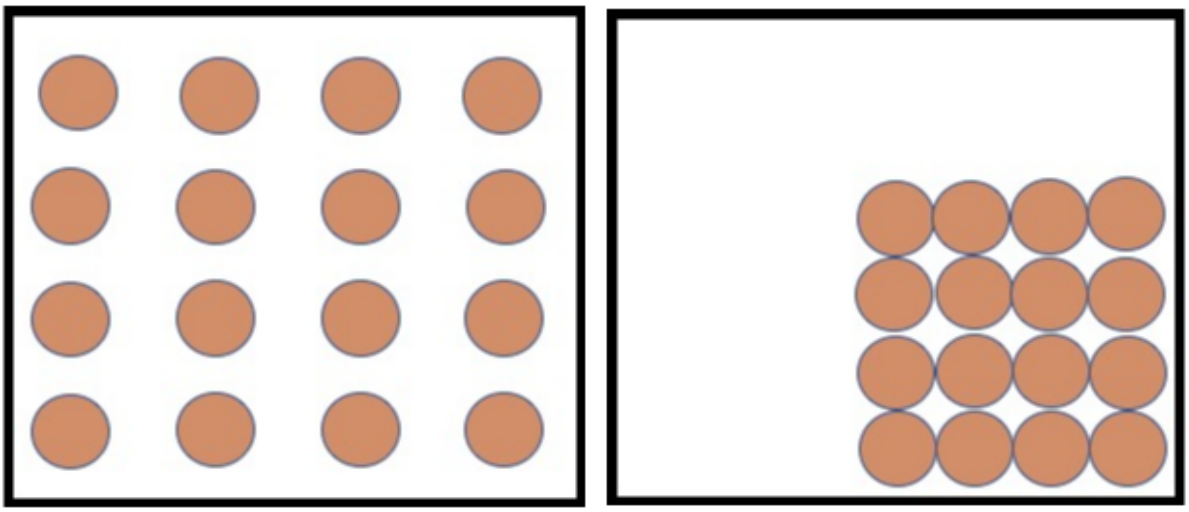

(a) (b)

Figure 4.1: Illustration of the difference in copper winding, of the coil in real life 4.1a and how COMSOL might interpret it 4.1b

4.1.2 Mechanics

To be able to simulate the mechanics of the transducer system, the most important part is to define the spring, and thereby the spring constant, k. The result for the spring constant can be seen in Table 4.1. The first value from the table shows the theoretical value of the spring constant given from equation 2.16. The resonance frequency used for the equation is given from measurements of a frequency response on the OMT. The second value in the table shows the measured spring constant given from a measurement of the OMT. The last value represents the simulated value of the spring, which is given by taking the derivative of the graph shown in Figure 4.2. Figure 4.2 shows the simulated displacement when a force was applied to the outer parts of the spring. As can be seen in the graph, the displacement is a linear reaction to the applied force.

Table 4.1: Table showing different spring constants given by theoretical calculations, measurements and simulation.

Theoretical spring constant (N/mm)	**Measured spring constant (N/mm)**	**Simulated spring constant (N/mm)**
k = 235.0	k = 277.0	k = 337.8

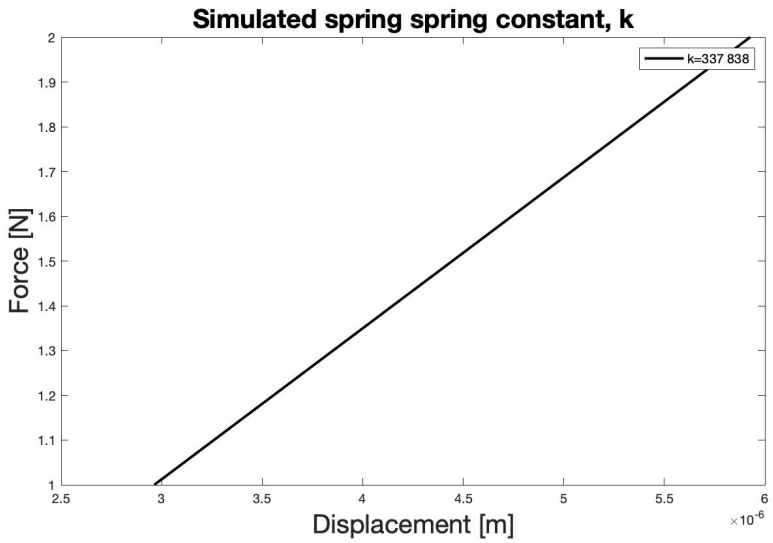

Figure 4.2: The displacement of the spring when applying an external force to the outer boundaries.

4.2 Case 2

The second case tests the stationary response from the system. This means the result will show $\boldsymbol{B}$, when the system is unable to move and the coil will be exposed to a DC current. The total $\boldsymbol{B}$ given from the simulation can be seen in Table 4.2. The table shows $\boldsymbol{B}$ in both the 2D and 3D model, in the four different measurement points. The magnetic field is the same for both the 3D and 2D model with some slight variations. Due to this similarity, only the 2D model is used in the next coming cases to decrease the computational cost.

Another result is that the total $\boldsymbol{B}$ given from the static simulation corresponds to the sum of $\boldsymbol{B}$ given from the permanent magnet and the coil. This is comparable to the results given from case 1. This means that the permanent magnet and the coil have the same polarity, and creating a flux in the same direction, when the model cannot move in this static, DC, case.

Table 4.2: The magnetic flux density of the stationary simulations in both 3D and 2D. The flux density is measured at four different points.

	Top of Bobbin Tower	**Bottom of Vibrator Plate**	**Middle of Bobbin Tower**	**Corner of Bobbin Tower**
Magnetic Field 2D	1.67T	1.63T	1.99T	2.56T
Magnetic Field 3D	1.57T	1.57T	1.94T	2.6T

How $\boldsymbol{B}$ is varied in the geometry can be seen in Figure 4.3. Figure 4.3a shows the distribution in the 2D model and Figure 4.3b in 3D. By comparing the results it is confirmed that the distribution is similar in 2D and 3D, verifying Table 4.2.

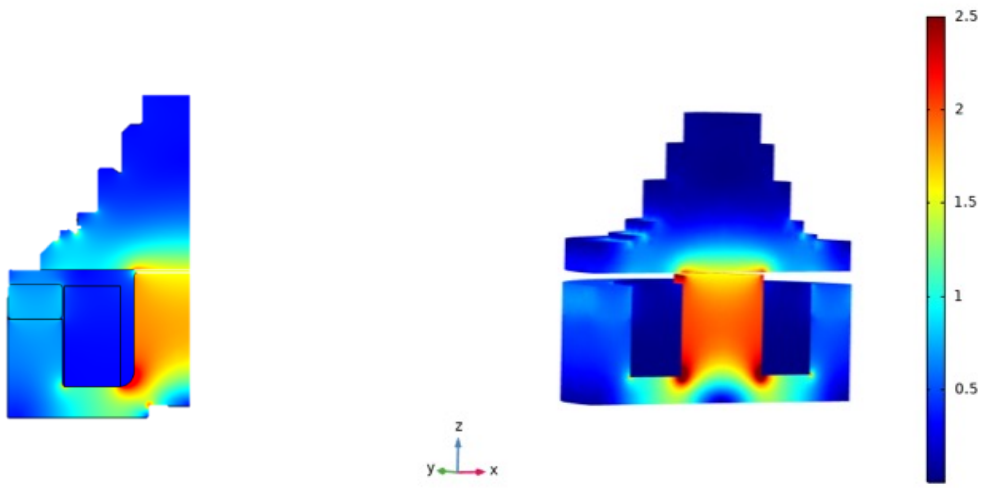

(a) Static field 2D (b) Static field 3D

Figure 4.3: The magnetic flux density in the 2D and 3D model.

To verify the strength of $\boldsymbol{B}$ and to ensure that the material parameters are working correctly, the saturation of the ferromagnetic material was simulated. As can be seen in Figure 4.4, the saturation of the cobalt-iron alloy used is around $2.28T$. This corresponds well with the datasheet for the cobalt-iron alloy, verifying the material properties. Since the magnetic field of the static simulation is $1.9T$ the material is not fully saturated, meaning that the air gap could possibly be reduced further to optimize the OMT.

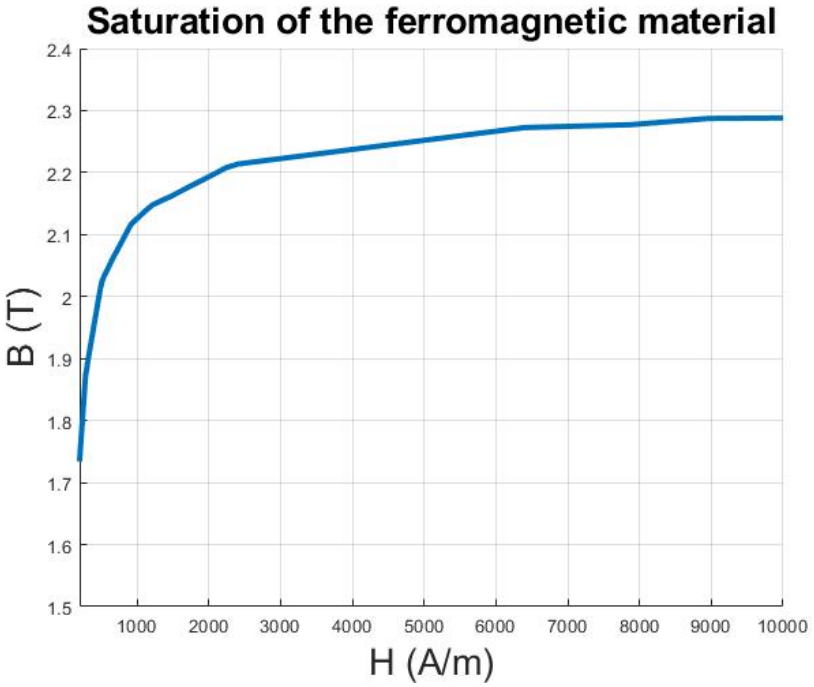

Figure 4.4: The saturation of the cobalt-iron alloy material, given by comparing the magnetic flux density to the magnetic field strength.

By analyzing the saturation of the cobalt-iron alloy, one can analyze the air gap limit for saturation of the magnetic field. Figure 4.5 shows the change in $\boldsymbol{B}$ when the air gap is being reduced. The measurements are performed in four different points, where the purple line indicates a measurement point in the corner of the bobbin tower, in which $\boldsymbol{B}$ is strongly enhanced. The blue line is a point in the middle of the bobbin tower which represents the overall magnetization of the bobbin tower. The orange line is a point on the top of the bobbin tower and the yellow is at the bottom of the vibrator plate. These two points should roughly have the same $\boldsymbol{B}$ since they are both at a similar distance from the coil and the permanent magnet. However, there should be a small difference in $\boldsymbol{B}$ since the two points are separated by the small air gap.

By looking at Figure 4.5, we can see that in the middle of the bobbin tower the material is saturated around $53\mu m$. This is shown by looking at for which air gap the blue line has a magnetic flux density of $2.28T$, which is the saturation given by Figure 4.4. However, as the figure shows there are areas in the ferromagnetic material that are not saturated. In the outer areas of the bobbin tower the material is not saturated until $44\mu m$ and in the corners saturation is given already at $110\mu m$. This shows that saturation of the material is different in different regions of the bobbin. However, since the middle point represents an arbitrary point of the magnetic flux in the bobbin, this is chosen as the lower limit of the saturation. Hence, the air gap that saturates the material in this measurement point is the lowest air gap the transducer can have before it is saturated. The air gap should also probably be slightly higher due to higher magnetic field in corner and other extreme points.

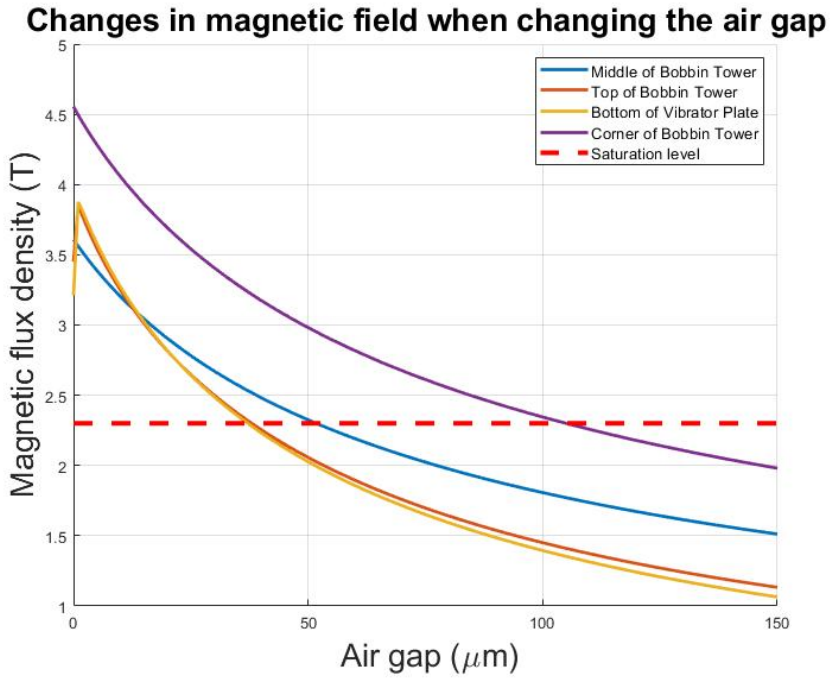

Figure 4.5: The magnetic flux density as a function of the air gap of the transducer. The graph also points out the saturation point of the material and at which air gap the measurements points are saturated.

4.3 Case 3

Case 3 shows the performance of the system in its entirety, which means the combination of magnetic fields and mechanics. The first result, seen in Figure 4.6, shows the mean value of 10 measurements of the OMT. The standard deviation for the mean is so small, that it cannot be represented in the graph. The largest value of the standard deviation is $0.3dB\mu N$. As can be seen, the resonance frequency is at $880Hz$ and the peak is $127.9dB\mu N$.

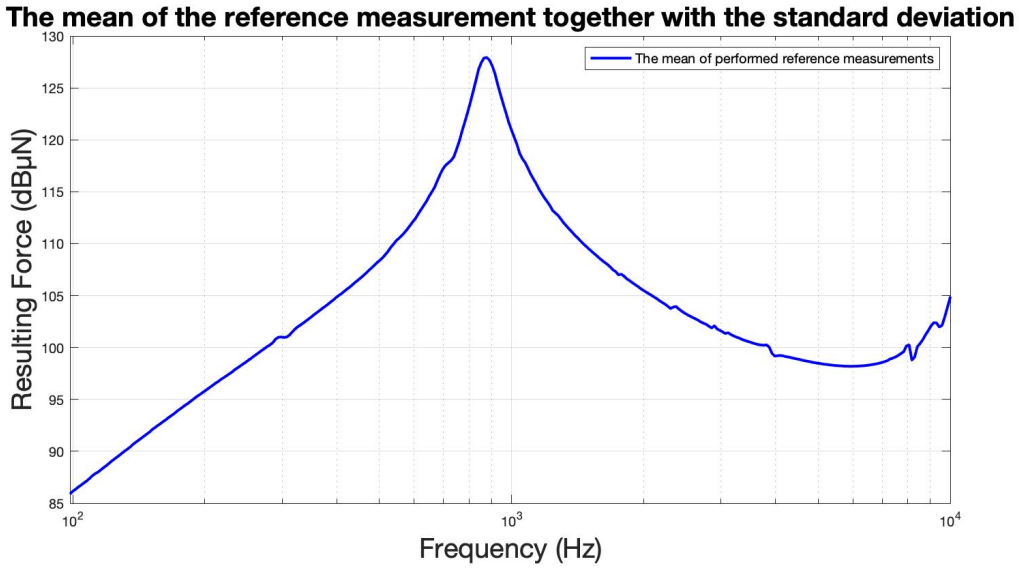

Figure 4.6: The force output as a function of frequency, calculated as the mean of ten measurements of an OMT. The force output is expressed in $dB\mu N$.

To be able to match the simulation to the measurements there are, as described in section 3.4, five parameters that can be changed to alter the behavior of the simulation. These parameters are the air gap of the transducer, the conductivity of the copper in the coil, the permeability of the cobalt-iron alloy used, the damping factor of the entire system and the spring constant. Figure 4.7 shows the correspondence of the system and the simulation when using the parameter settings given by previous cases. This means the given spring constant from case 1 and the same air gap used for the previous simulations. The damping factor was set to an approximated value which only guaranteed the damping ratio described in equation 2.15 to be between zero and one, as the system is minimally damped. These parameter settings can be seen in Table 4.3. As can be seen in Figure 4.7 the simulation is shifted to the right, with a higher resonance frequency, higher peak and lower output in the lower frequency region. This means the first simulated parameters were a bad fit with the specific OMT that was investigated. Since the simulation is highly shifted in frequency with the resonance peak, the biggest problem concerns the spring constant.

Table 4.3: The parameter settings for the first simulation of case 3. The parameters are given from case 1.

Airgap	**Conductivity**	**Permeability**	**Damping factor**	**Spring constant**
$75\mu m$	$6 \cdot 10^7 S/m$	1000	2	$337[N/mm]$

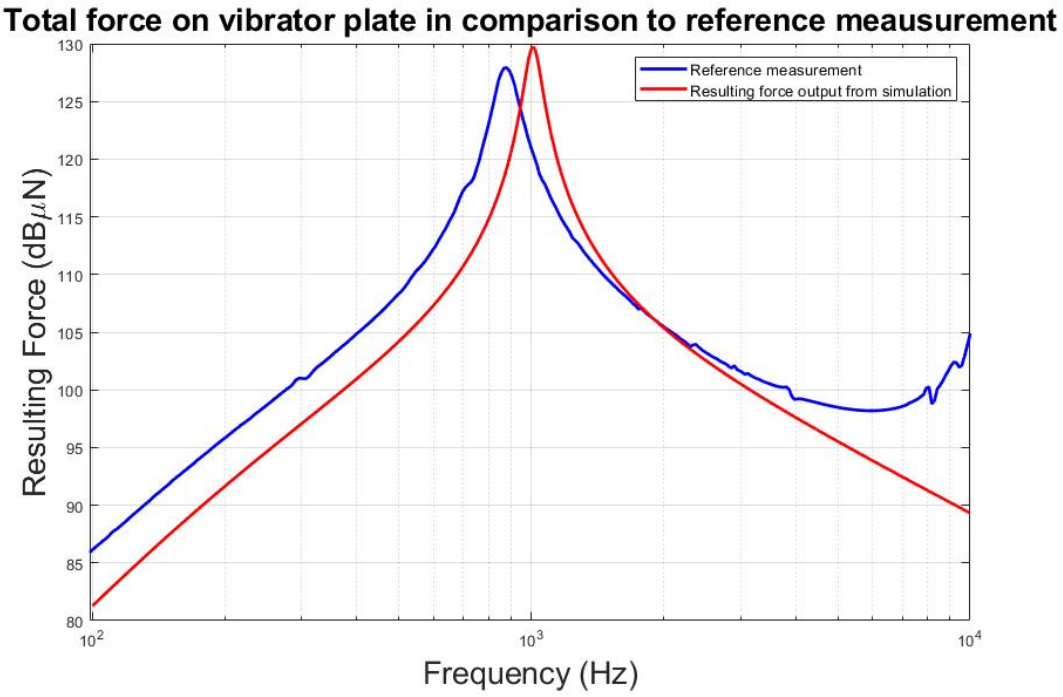

Figure 4.7: The force output from the reference measurement and from the simulation, using the parameter settings from case 1.

To be able to create a more matched simulation, an effort was made to try and match the resonance peak of the simulation and reference measurement. The effect of this was that the spring constant needed to be changed together with the air gap. The updated parameter settings can be seen in Table 4.4. The result from these parameter settings can be seen in Figure 4.8. By changing the spring constant and the air gap, the simulation seem at first hand to fit fairly well to the reference measurement. However, at a second glance the simulated force output is too high in both the frequency span $400Hz - 800Hz$ and the $900 - 3000Hz$. Since these frequencies are part of the more important areas, which could be seen in section 2.1 it means the simulation needs to be altered further.

Table 4.4: The parameter settings of the second simulation attempt.

Airgap	**Conductivity**	**Permeability**	**Damping factor**	**Spring constant**
$69.4\mu m$	$6 \cdot 10^7 S/m$	1000	1.2	$270[N/mm]$

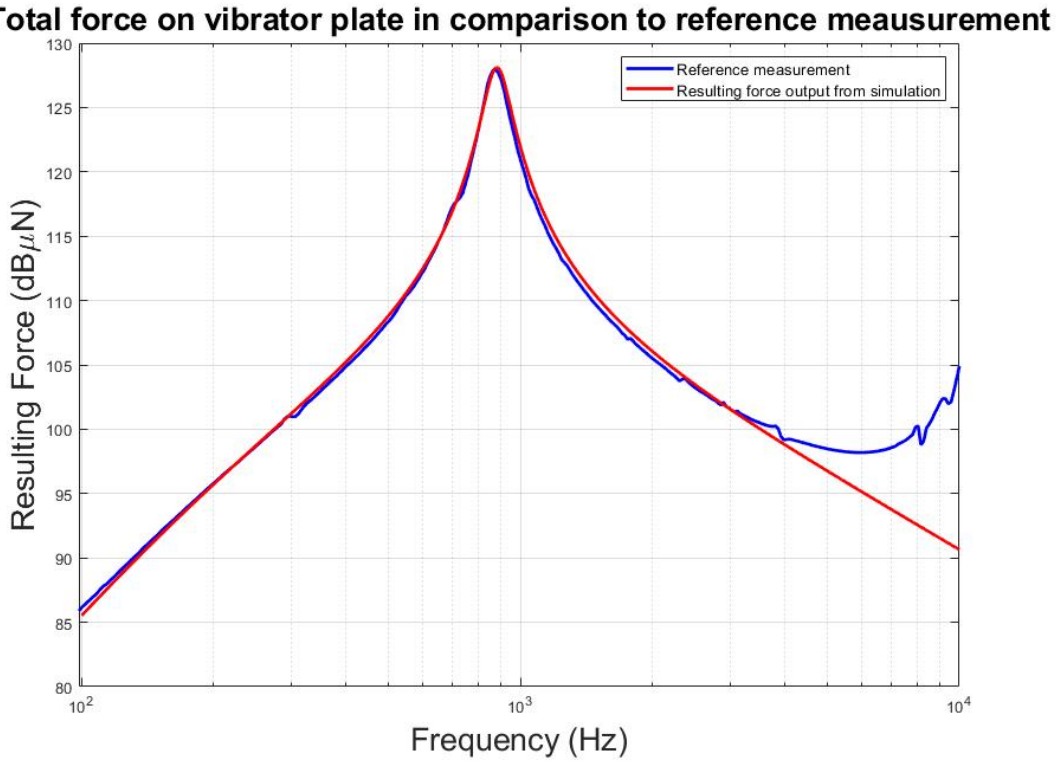

Figure 4.8: The matched simulation in regards to resonance.

The higher frequency span is difficult to match with the simulation since there are no parameters only affecting this. However, the lower frequency span can be affected by changing the conductivity. Since the response of the simulation is too high at $400Hz$, this means that copper conductivity needs to be decreased. This corresponds well to the result given from case 1 where the conductivity needed to be decreased to match the measured resistance of the coil. By changing the conductivity of copper to $5.26 \cdot 10^7 S/m$, the simulation is almost identical to the reference measurement, which can be seen in Figure 4.9. The biggest differences here are in the lowest frequency span of $100 - 200Hz$, in the resonance peak and in the upper frequency span, from $4000 - 10000Hz$. The resonance peak can be matched further by alternating the damping factor. However, it was determined that the simulation was as similar to the reference measurement as needed.

Table 4.5: The final parameter setting for the OMT.

Airgap	**Conductivity**	**Permeability**	**Damping factor**	**Spring constant**
$69.4\mu m$	$5.26 \cdot 10^7 S/m$	1000	1	$270[N/mm]$

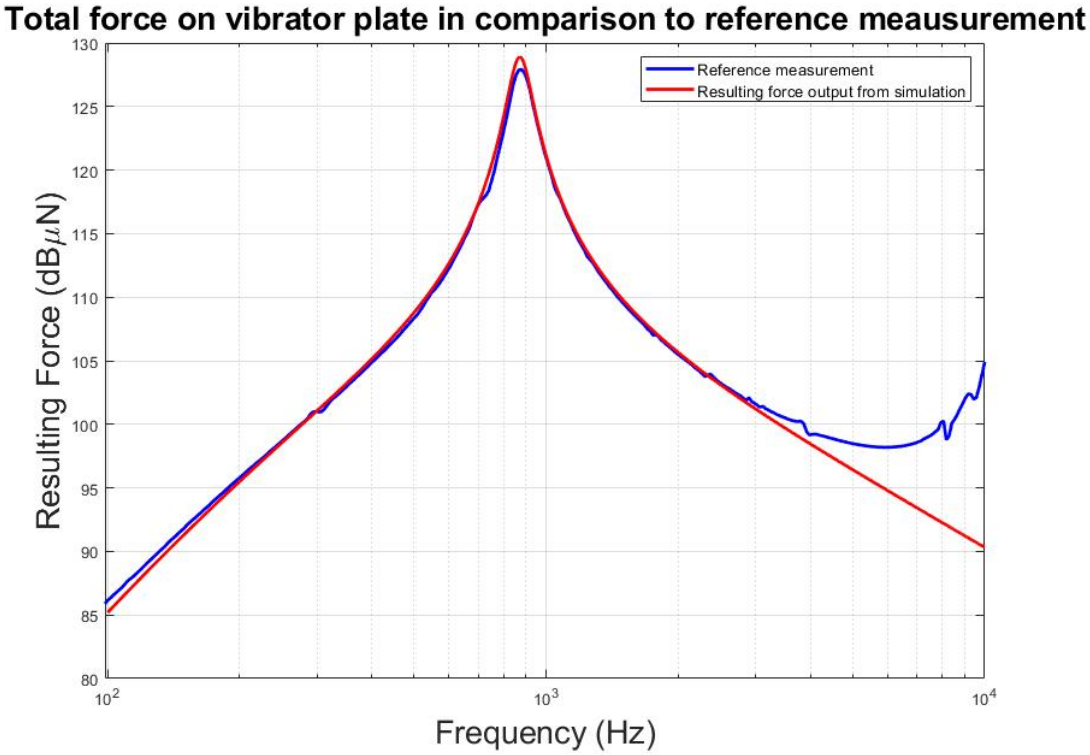

Figure 4.9: The force output from the reference measurement and from the simulation, using the final parameter settings.

When the final parameter settings for the system had been confirmed, the maximum displacement of the moving mass could be analyzed. Figure 4.10 shows the absolute value of the displacement of the moving mass, with regards to frequency. The figure shows that the maximum displacement, which occurs at resonance frequency, is $17.5\mu m$. This is how far from the equilibrium point, at $69.5\mu m$, the moving mass will oscillate. By subtracting the displacement from the equilibrium point the minimum air gap of the dynamic transducer is given at $52\mu m$. This is below the saturation limit given from the second case, but since this only occurs at resonance the transducer will not be saturated for other frequencies.

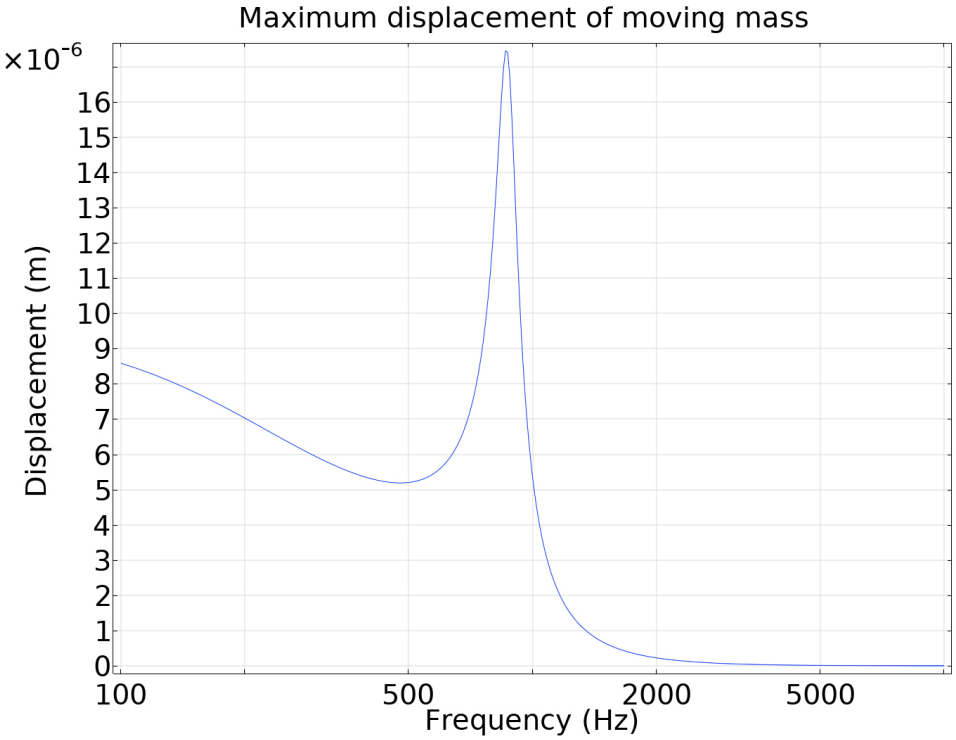

Figure 4.10: Maximum displacement of the moving mass from its equilibrium point of 69.4μm.

4.4 Case 4

As mentioned in section 3.4, the purpose of the fourth case was to optimize the OMT in regards to how different attributes would affect the force output. The three attributes studied are the permeability of the ferromagnetic material, the magnetization vector of the permanent magnet and different air gaps.

To compare the effects of the permeability, the magnetization vector and air gap was fixed. The results can be seen in Figure 4.11, which illustrates that the permeability of the ferromagnetic material has low impact on the force output. When simulating the different permeabilities a linear relative permeability model was used, instead of the B-H model. The reason was that the B-H model in COMSOL alters the permeability depending on the B-H plane, which was not desired when investigating the permeability. The permeability was instead defined as a parameter. This model prevents saturation of the material.

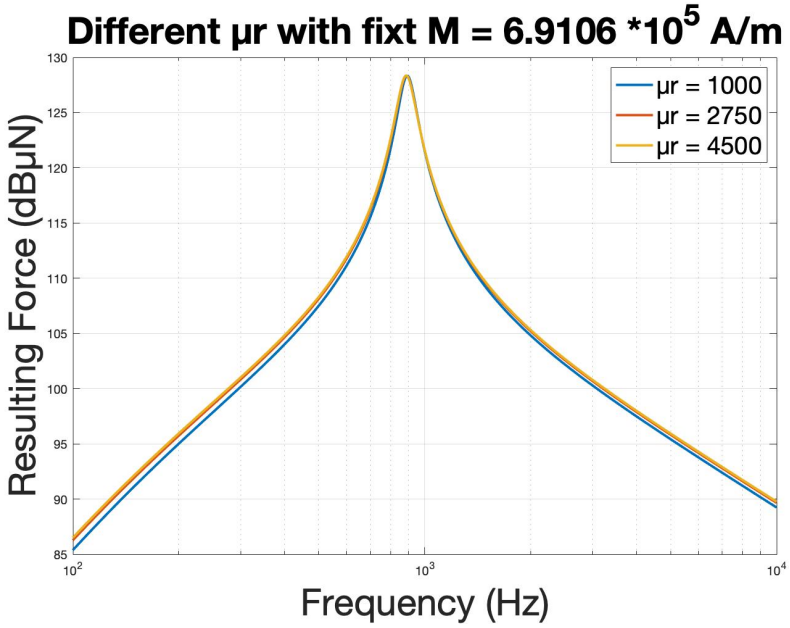

Figure 4.11: Force output for different permeabilities in the ferromagnetic material.

In Figure 4.12 the simulated magnetization vectors can be seen. The figure indicates a strong correlation between the magnetization vector and the force output. The yellow line, corresponding to the highest magnetization vector, has reached saturation. This can be seen as the force output for lower frequencies is decreasing compared with the lower magnetization vectors, the red and the blue line. In order to compensate for this, the air gap can be increased as this would decrease the magnetic flux passing through the air gap to the vibrator plate.

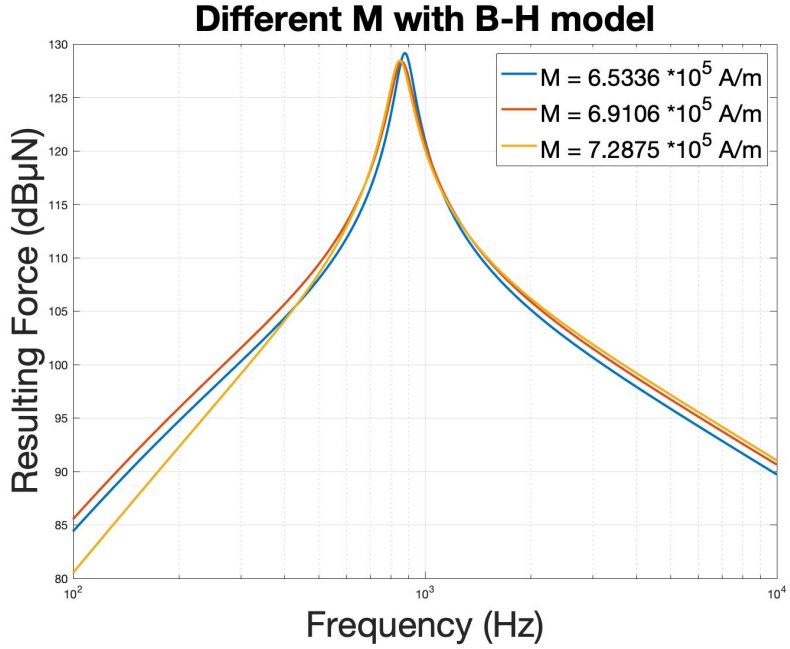

Figure 4.12: Force output for different magnetization vectors defining the permanent magnet.

To test how changing the air gap affected the force output, several air gaps were simulated.

Figure 4.13 shows the force output when the air gap of the transducer was changed from $150\mu m$ to $80\mu m$. The stated air gaps would result in the air gaps given by Table 3.6 when affected by the static magnetic field. The results are divided in two, where Figure 4.13a shows the air gaps where the transducer is not yet saturated. This corresponds to the larger air gaps, where a smaller air gap is corresponding to a higher force output as the magnetic flux in the air gap is increasing, related to equation 2.12. However, when looking at the resonance frequency we can see that the force output is decreasing with smaller air gaps, meaning that saturation can be an issue in resonance. The second figure, Figure 4.13b, shows the air gaps that result in saturation. This can be seen when a smaller air gap results in a lower force output. Some shifting can be seen in the resonance frequency which also indicates saturation. The smallest air gap before saturation was found to be 64.51 μm, which is larger than the air gap suggested in case 2. However, this can be explained due to the vibrations that occurs when the transducer can move and the OMT vibrates around 17.5 μm, meaning that the OMT is vibrating into saturation if the air gap is 53 μ, as suggested in case 2. An interesting effect to point out, is that even though the air gap is decreased linearly the resulting working point is not. This is due to the non linear magnetic force exerted by the permanent magnet and is the reason to why the air gaps are increasing more and more for each simulation.

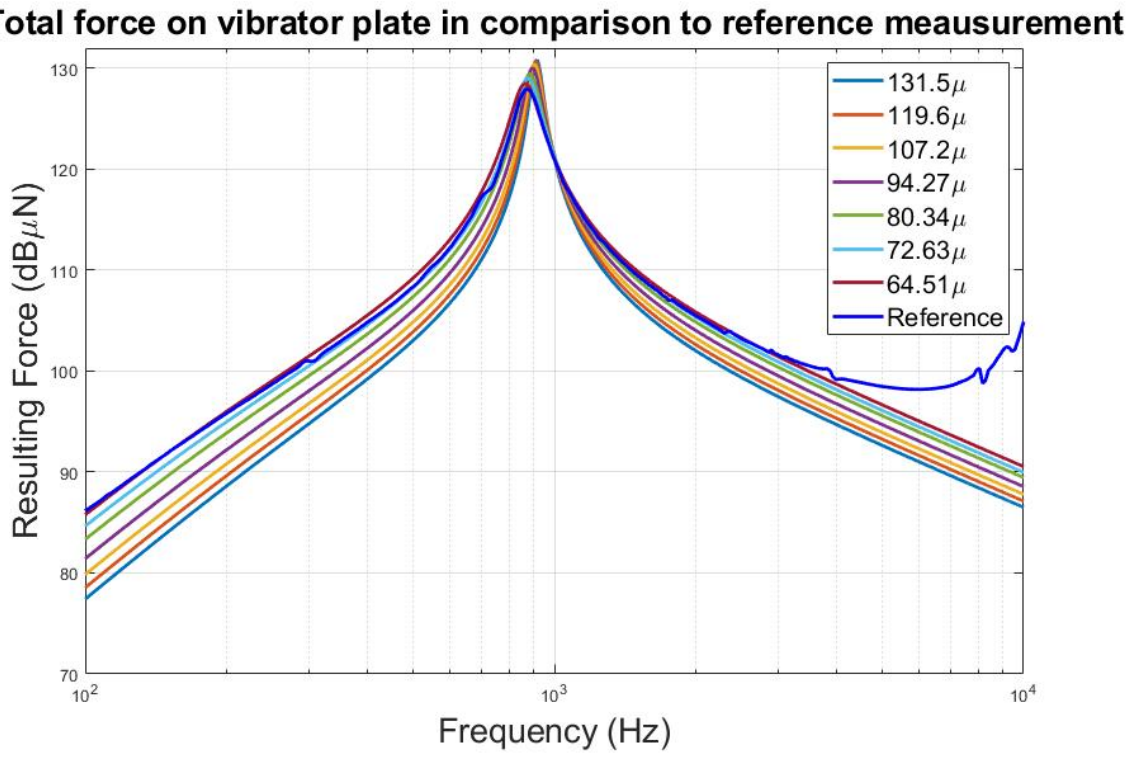

(a) Different air gaps before saturation

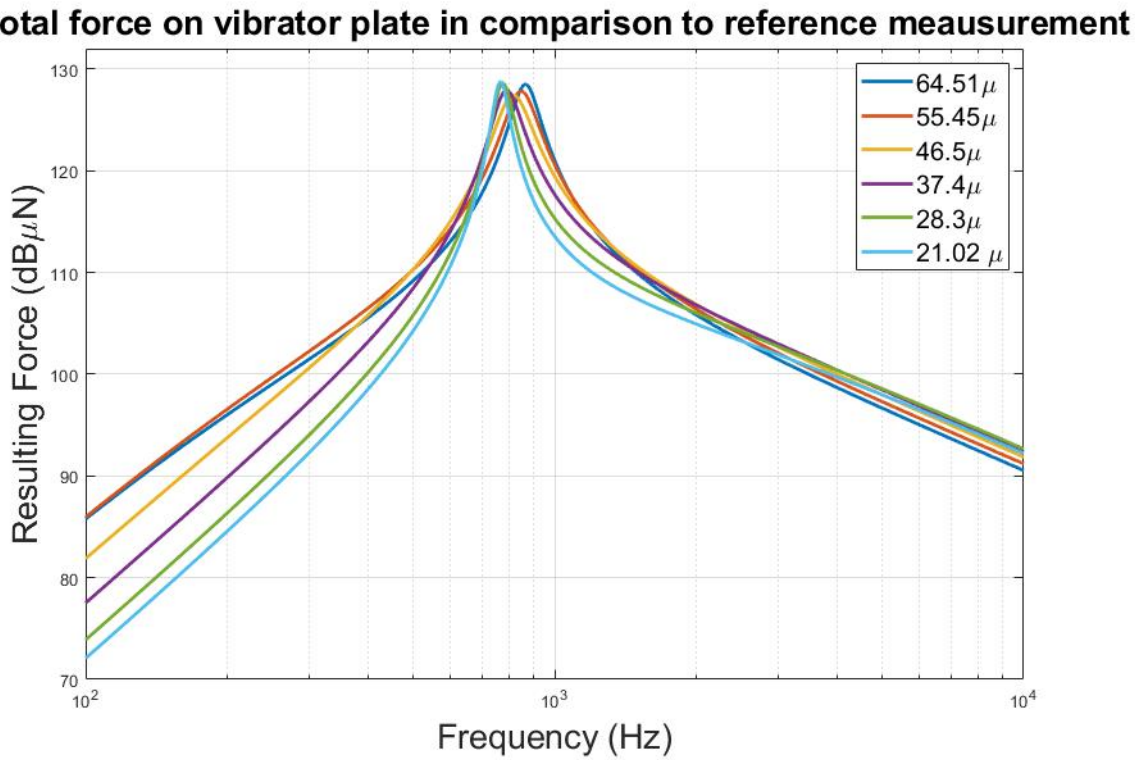

(b) Different air gaps during saturation

Figure 4.13: The effects on the force output, of decreasing the air gap of the transducer.

5

Discussion

In the discussion section, each of the previous cases will be presented. Here the results from each section as well as the method for obtaining them will be discussed. The last section of the discussion presents what could be done to further expand the study.

5.1 Case 1

As can be seen in Table 4.1 the values of the spring constants differ from each other, which might be due to the difficulty of estimating the spring constant. The theoretical spring constant does not take into account the damping of the system and other effects caused by for example friction and other physical properties. The simulated spring constant is instead affected by where on the spring the displacement is measured. It will also differ from the real value due to geometrical alterations of the spring from welding. The reason behind this is that laser welding means that the fastening of the spring edges are not as well defined as in the simulation model. This means the theoretical and simulated values for the spring constant mark the upper and lower boundary of the spring constant and that the measured spring constant should be in between. Since the displacement of the spring differs depending on if it is measured on for example the edge of the spring or in the middle. This is due to its complexity and the spring constant is now extracted from a surface average of the outer edge. If a more complex model was developed the spring constant could be calculated in each iteration. However, this would significantly increase computational cost in the model whilst only slightly contributing to the results.

As can be seen in Figure 4.1b and 4.1a, the winding of the copper coil might differ in the simulation compared with the reference measurement. The reason was different coil resistance between the simulation and the reference measurement. The resistance in the coil is dependent on the length of the copper winding, meaning that a higher resistance implies a longer copper thread. The different length could be a result of a perfect isolation in the simulation, whilst this is impossible to achieve in real life. In order for the copper to get the correct characteristics the conductivity of the copper wire is adapted so that the resistance of the measurements matches the resistance of the reference measurement.

5.2 Case 2

When analyzing the static simulations, a difference between the 2D and 3D simulation was found, that was not initially expected. The reason for this difference could be that

the evaluation points are not exactly placed at the same coordinates, leading to this small variation. Another possible difference is the definition of the coil in 2D compared with 3D, that appears in COMSOL. When defining the coil in 3D, the circulation of the induced currents needs to be defined, while this three dimensional circulation is not possible in a 2D model. To confirm this, it would have been possible to test the permanent magnet to make sure it gave the same magnetic flux in both 3D and 2D. However, as the results implies, this variation is small with a maximum difference of $< 0.1T$ which is why this is not considered an issue and why it was not more thoroughly examined.

The results from case 2 which defines the air gap before saturation to be at the minimum value of $53\mu m$, was based on the saturation level of $2.28T$ which was the value given from simulation. According to the datasheet of cobalt-iron alloy, the material saturates at $2.3T$. Which means the material will saturate at $51\mu m$ instead. However, the resolution of the datasheet is unknown and since the difference in result is fairly low, this was estimated to be a low error margin.

5.3 Case 3

Case 3 was designated to create a simulation environment in which the simulated force output would be fully comparable to the real force output from the reference measurement. To be able to achieve this a choice was made regarding creating a simplified version of the model using ODE or if it was possible to simulate the entire transducer using material parameters. As can be seen in the results, the simplified version gives a satisfying result. This shows that even though the simulation only solves one ODE and negates movement in all direction but the z-direction, it still performs as required. The benefits of creating this simplification is that it is saving a huge amount of computational cost and reduces the simulation time.

However, one could argue that the result would be even more realistic if the simulation was done entirely with solid mechanics and material parameters. This would create a more complex model, but an issue might be that the model is instead over determined. The downside of a more complex model is always the increase in computational cost and simulation time. Therefore, since the used model performed with the caliber it did, there is no reason to create a more complex model. However, this simulation is strictly limited to magnetic fields, meaning if heating or other secondary effects would have to be included in the simulation, a more complex model is needed. Another benefit of using a 3D model is that asymmetrical movement of transducer can also be investigated and also component that are not axisymmetric.

An interesting aspect to comment on is the result given from Figure 4.8. In this graph the results from the simulation seem to be more suited to the reference measurement, than the actual chosen simulation result from Figure 4.9. However, it is noticeable that the simulation fits better at the resonance peak and that the force output is too high in the regions from $400Hz - 800Hz$ and $1000 - 3000Hz$. Due to this the decision was made to fit the simulation better to the lower and higher frequency span, since this is a larger frequency span for human speech. The decision to lower the copper conductivity was also based on the result from case 1, which is also one of the reasons to why it was made. However, since regions below $400Hz$ also is part of the human speech spectrum,

one could argue that there was no reason to lower the copper conductivity of the coil. By decreasing the conductivity in the material it could be seen that the simulation was too low in frequencies below $400Hz$ and in $3000Hz$. However, it is more matched in the frequencies ranging from resonance to $3000Hz$

A problem which can be seen in all studies in case 3 is that the reference measurements deviates from the simulations in higher frequencies. The simulation is declining in a logarithmic fashion, whilst the reference measurements starts to decline less. The culmination of this can be seen at $10000Hz$ where the reference measurements start to oscillate. The reason behind this is due to the connection to the skull simulator, to which the OMT is attached to measure its force output. At higher frequencies, where the transducer vibrates rapidly, the mechanical attachment introduces a resonance meaning the force output is not dropping as rapidly. This can be simulated by attaching another spring mass system to the vibrator plate, instead of just assuming the top of the vibrator plate is rigid. However, this adds complex calculation which were deemed outside this projects scope.

5.4 Case 4

As described in section 3, there are two different models used to simulate the permeability of the ferromagnetic material. When the permeability of the material could vary, a $\boldsymbol{B}-\boldsymbol{H}$ plane model generated in COMSOL was used. This was preferred as it provides sufficient results regarding saturation. However, when investigating the given, fixed permeabilities, a linear relative permeability model was used. The results indicates that the impact of the permeability in the ferromagnetic material has small impact on the force output and saturation of the OMT. If a non-linear model was used instead the results may differ, but as the permeability changes when a material is saturated it might instead be of interest to investigate how it affects the force output before saturation, when the permeability is acting linearly. Then, the linear permeability can be seen to have a small impact on the force output, seen in Figure 4.11.

5.5 Future work

To be able to further investigate simulations of electromechanical systems, the first things which could have been altered are some of the limitations. For example this study is limited to having movement only in the z-direction in the transducer. This means no rotational force is taken into consideration and a simplification of the real life transducer is being used. So to further investigate the behavior of the system a more complex model can be used. Another problem with the simplifications is the use of a 2D-model. The prerequisites of using a 2D model is that the components of the system are axisymmetric. Hence, components such as the spring, of the transducer, can't be simulated. It is also impossible to simulate optimization aspects which will result in components becoming non axisymmetric, such as creating an angled air gap or removing material from one side. The effects of these optimization suggestions can be interesting to analyze which means a more complex model can be needed.

In regards to the optimization of the transducer, simulation is a powerful tool to be used.

For future works the fourth case of this thesis could be expanded. The thesis was limited to only investigating three parameters, where there are more existing possibilities. For example, one could investigate the change in size of some components, by removing or adding material. However, this was beyond the scope of this project since it was more important to create and afterwards tune the model of the transducer. Even though the simulations can be applied on multiple BC transducers, they might not work on all. Examples on where the simulation needs to be redesigned is the BEST transducer, as this transducer is designed differently [17].

Another method that could be used to evaluate a BC transducer is by the use of machine learning. This has been previously done in a master´s thesis in collaboration with Cochlear Bone Anchored Solutions [32]. The thesis concludes that machine learning was successfully implemented to predict the gain values of the BAHS and could possibly be a complement to the simulations conducted in this thesis. Another study in a similar area is one performed by R. Dhaylan and K. Balusbramaniam which investigates FEM simulations for electromagnetic acoustic transducers [33]. In this case, similarly to our project, a 2D model was created to simplify the earlier stages of simulation. However, this study aimed at looking at transducer in a time-frequency analysis and on a different kind of transducer, which in the end makes it differ from this project.

6

Conclusion

The main conclusion from the thesis is that a simulation environment is an effective method to evaluate an OMT, and more generally multiple versions of BAHS transducers. This can be in regards to simulation of the electromagnetic flux through the transducer, to find weak spots where the material is saturated or to optimize the transducer. Another conclusion is that a 2D environment is to be preferred when possible. This is due to less computational cost for the 2D simulation compared with the 3D simulation while the results provided are similar.

Even though the simulations used a simplified model with global ODE:s, it still gave a reasonable result. By making some simplifications, the computational cost is significantly reduced. This means that the gain in computational cost would outweigh the possible gain in sensitivity by creating a more complex model. Hence, it is not always most beneficial to create a more complex model.

The magnetization vector and the magnetic dipole moment of the permanent magnet have been shown to have an impact on the saturation of the material. The conclusion is that the air gap, as expected, on different OMT:s should vary in order to get the same force output depending on the magnetization of the permanent magnet. It can also be concluded that a relative linear permeability model can not be used to simulate saturation effects and that a fixed permeability has a low impact on the force output in comparison to the static magnetization.

The simulations shows that it is possible to optimize the OMT in regards to different air gaps given the magnetization vector. The minimal possible air gap before saturation was simulated to 64.51 μm, and it is possible to see the results of having both increased or decreased air gaps.

It is also concluded that the simulation can be used as an effective method to investigate behavior and properties that are hard to measure in real life. The conducted simulations fulfill its aim to provide electromechanical simulations for an OMT.

References

[1] World Health Organization, "Addressing the rising prevalence of hearing loss", Tech. Rep. 1, 2018, p. 159. DOI: 10.1080/09687599.2011.589198. arXiv: NBK304079. [Online]. Available: https://apps.who.int/iris/bitstream/handle/10665/260336/9789241550260-eng.pdf?sequence=1{\&}ua=1{\%}0Ahttp://www.hear-it.org/multimedia/Hear{_}It{_}Report{_}October{_}2006.pdf{\%}0Afile:///C:/Users/E6530/Downloads/9789240685215{_}eng.pdf{\%}0Ahttp://dx.doi.org/10.1016/j.ijporl.

[2] Hearing Loss Association of America, *Hearing loss: Types, Causes and Treatment*, 2019. [Online]. Available: https://www.hearingloss.org/hearing-help/hearing-loss-basics/types-causes-and-treatment/ (visited on 02/18/2020).

[3] J. Victory, *Hearing Loss*, 2019. [Online]. Available: https://www.healthyhearing.com/help/hearing-loss (visited on 02/18/2020).

[4] J. B. Nadol, "Hearing Loss", *The New England Journal of Medicine*, vol. 329, no. 15, pp. 1092–1102, 1993.

[5] B. Håkansson, A. Tjellström, U. Rosenhall, and C. Peder, "The Bone-Anchored Hearing Aid: Principal Design and a Psychoacoustical Evaluation", *Acta Oto-Laryngologica*, vol. 100, no. 3-4, pp. 229–239, 1985. DOI: 10.3109/00016488509104781.

[6] Oticon Medical, *Ponto 3*, 2020. [Online]. Available: https://www.oticonmedical.com/us/info/ponto3 (visited on 02/18/2020).

[7] D. Williams, *Sound Detection*. 2019, pp. 42–69, ISBN: 0309545145. DOI: 10.4324/9780429201912-3.

[8] G. J. Tortora and B. Derrickson, *Introduction to the Human Body*, Tenth edit. United States of America: John Wiley & Sons, 2015, pp. 286–292, ISBN: 978-1 118-58318-0.

[9] L. Chittka and A. Brockmann, *File: Anatomy of the Human Ear*. [Online]. Available: https://upload.wikimedia.org/wikipedia/commons/d/d2/Anatomy{_}of{_}the{_}Human{_}Ear.svg (visited on 05/20/2020).

[10] A. Möller and A. R. Möller, *Hearing : Anatomy, Physiology, and Disorders of the Auditory System*, Third Edit. Plural Publishing, Incorporated.

[11] K.-J. Fredén Jansson, "The Balanced Electromagnetic Separation Transducer for Bone Conduction Audiometry and Hearing Rehabilitation", Thesis for the degree of Doctor of Philosophy, Chalmers University of Technology, 2017, pp. 7–10.

[12] S. Reinfeldt, "Bone Cnduction Hearing in Human Communication Sensitivity, Transmission and Applications", Thesis for the degree of Doctor of Philosophy, Chalmers University of Technology, 2009, p. 3.

[13] J. Guo, R. Chai, H. Li, and S. Sun, *Hearing Loss: Mechanisms, Prevention and Cure*, Ci. 2019, vol. 1130, pp. 17–36, ISBN: 978-981-13-6122-7. DOI: 10.1007/978-981-13-6123-4. [Online]. Available: http://link.springer.com/10.1007/978-981-13-6123-4.

[14] S. Reinfeldt, B. Håkansson, H. Taghavi, and M Eeg-Olofsson, "New developments in bone-conduction hearing implants: a review", *Dovepress*, vol. 2015:8, pp. 79–93, 2015. DOI: https://doi.org/10.2147/MDER.S39691. [Online]. Available: https://www.dovepress.com/new-developments-in-bone-conduction-hearing-implants-a-review-peer-reviewed-article-MDER.

[15] H. Taghavi, "The Bone Conduction Implant (BC)", Thesis for the degree of Doctor of Philosofy, Chalmers University of Technology, 2014.

[16] Cochlear, *Baha - Bone conduction implants*, 2020. [Online]. Available: https://www.cochlear.com/sv/home/discover/baha-bone-conduction-implants (visited on 05/10/2020).

[17] B. Håkansson, "The balanced electromagnetic separation transducer: A new bone conduction transducer", *Acoustical Society of America*, vol. 113 (2), 2003. DOI: 10.1121/1.1536633.

[18] D. K. Cheng, *Field and Wave Electromagnetics*, Second. Edinburgh: Pearson, 2014, pp. 225–294, ISBN: 13:978-1-292-02656-5.

[19] D. Jones, *The Theory of Electromagnetism*. London: Pergamon Press ltd, 1964. [Online]. Available: https://books.google.se/books?hl=sv{\&}lr={\&}id=9aBGBQAAQBAJ{\&}oi=fnd{\&}pg=PP1{\&}dq=electromagnetism{\&}ots=uvTUOBUqH1{\&}sig=Ey2BQwuzw1VMDw1Hag0ol9cMq1w{\&}redir{_}esc=y{\#}v=onepage{\&}q=electromagnetism{\&}f=false.

[20] J. Clarke Slater and N. H. Frank, *Electromagnetism*. Massachusetts: Dover publicantions, INC, 1969.

[21] J. O. Bird and P. J. Chivers, "Electromagnetism and magnetic circuits", in *Newnes Engineering and Physical Science Pocket Book*, 1993. DOI: 10.1016/b978-0-7506-1683-6.50013-8.

[22] B. Håkansson, "Technical Report Nr. 759.pdf", Chalmers University of Technology, Göteborg, Tech. Rep., 1984.

[23] J. W. Jewett and R. A. Serway, *Physics - For Scientists and Engineers with Modern Physics*, 7th ed. United States of America, 2008, ISBN: 0-495-11250-2.

[24] B. Lennartson, *Reglerteknikens grunder*, 4th ed. Studentlitteratur AB, 2002.

[25] T. Johansson, *Private communication with Oticon Medical*, Göteborg, 2020.

[26] D. V. Knudson, *Fundamentals of Biomechanincs*. New York: Kluwer Academic/-Plenum Publisher, 2002. [Online]. Available: https://books.google.se/books?id=js2P{_}8lbR2wC{\&}pg=PA134{\&}dq=newton{\%}27s+second+law{\&}hl=sv{\&}sa=X{\&}ved=0ahUKEwj6-LTSzoPqAhVo16YKHS55C34Q6AEIMTAB{\#}v=onepage{\&}q=newton'ssecondlaw{\&}f=false.

[27] D. H. Norrie, *A first course in the finite element method*, 2. 1987, vol. 3, pp. 162–163, ISBN: 0534552986. DOI: 10.1016/0168-874x(87)90008-4.

[28] R. A. Adams and C. Essex, *Calculus: A Complete Course (7th Edition)*, Toronto, 2009. [Online]. Available: http://www.pdf177.com/pdf/calculus-complete-course-pdf-83705.pdf.

[29] Comsol, *Understand, Predict, and Optimize Physics-Based Designs and Processes with COMSOL Multiphysics*, 2020. (visited on 02/11/2020).

[30] D. Ralph, "GLOBAL CONVERGENCE OF DAMPED NEWTON'S METHOD FOR NONSMOOTH EQUATIONS VIA THE PATH SEARCH", *MATHEMATICS OF OPERATIONS RESEARCH*, vol. 19, no. 2, pp. 352–389, 1994.

[31] Vacuumschmelze, "Cobolt-iron alloys", 2002, [Online]. Available: https://www.vacuumschmelze.com/Products/Soft-Magnetic-Materials-and-Stamped-Parts/49-Cobalt-Iron---VACOFLUX-and-VACODUR.

[32] R. T. Sebastian, "Prediction of the gain values produced by a Bone Anchored Hearing Aid (BAHA) using Machine Learning", Master´s thesis, Chalmers University of Technology, 2019. [Online]. Available: https://odr.chalmers.se/bitstream/20.500.12380/300633/1/Sebastian{_}2019.pdf.

[33] R Dhaylan and K. Balasubramania, "A hybrid finite element model for simulation of electromagnetic acoustic transducer (EMAT) based plate waves", *NDT & E International*, vol. 43, no. 6, pp. 519–526, 2010.